

SURFACE PHOTOMETRY OF NEARBY FIELD GALAXIES: THE DATA

ROLF A. JANSEN^{1,2}, MARIJN FRANX^{1,3}, DANIEL FABRICANT², & NELSON CALDWELL^{4,2}

¹Kapteyn Astronomical Institute, Postbus 800, NL-9700 AV Groningen, The Netherlands

²Harvard-Smithsonian Center for Astrophysics, 60 Garden St., Cambridge, MA 02138

³Leiden Observatory, Postbus 9513, NL-2300 RA Leiden, The Netherlands

⁴F.L. Whipple Observatory, Amado, AZ 85645

jansen@astro.rug.nl, franx@strw.leidenuniv.nl, dfabricant or ncaldwell@cfa.harvard.edu

Received 1999 May 5; accepted 1999 August 19

ABSTRACT

We have obtained integrated spectra and multi-filter photometry for a representative sample of ~ 200 nearby galaxies. These galaxies span the entire Hubble sequence in morphological type, as well as a wide range of luminosities ($M_B = -14$ to -22) and colors ($B-R = 0.4$ to 1.8). Here we describe the sample selection criteria and the U, B, R surface photometry for these galaxies. The spectrophotometric results will be presented in a companion paper. Our goals for the project include measuring the current star formation rates and metallicity of these galaxies, and elucidating their star formation histories, as a function of luminosity and morphology. We thereby extend the work of Kennicutt (1992) to lower luminosity systems. We anticipate that our study will be useful as a benchmark for studies of galaxies at high redshift.

We discuss the observing, data reduction and calibration techniques, and show that our photometry agrees well with previous work in those cases where earlier data are available. We present an atlas of images, radial surface brightness profiles and color profiles, as well as tables of derived parameters. The atlas and tables of measurements will be made available electronically.

We study the correlations of galaxy properties determined from the galaxy images. Our findings include: (1) colors determined within the effective radius correlate better with morphological type than with M_B and (2) 50% of the low luminosity galaxies are bluest in their centers.

Subject headings: cosmology: galaxy population — galaxies: surface photometry — galaxies: fundamental parameters — galaxies: nearby — galaxies: surveys,atlases

1. INTRODUCTION

With the advent of the Hubble Space Telescope, 8-m class ground-based telescopes, and effective new instruments, it is now possible to study the colors, morphologies and spectra of large samples of distant, faint galaxies. Frequently, our interpretation of such data is limited by the scarcity of good comparison samples in the local universe. Because distant galaxies subtend angles comparable to spectrograph slit widths, we usually obtain integrated spectra, while the same slits sample only the nuclear regions of nearby galaxies. This observational issue complicates the comparison of distant and nearby galaxy spectra.

In a pioneering effort, Kennicutt (1992ab) obtained integrated spectrophotometry for 90 galaxies spanning the entire Hubble sequence. This study has had broad application for the study of galaxy spectral properties at both high and low redshift. Kennicutt's study, however, is limited to the brightest galaxies of each morphological type, and no uniform, multiple fil-

ter, surface photometry is available for these galaxies. Also, only half of Kennicutt's sample of 90 galaxies was observed at 5–7 Å spectral resolution by trailing the image of a galaxy across a long slit. The remaining half was observed at 15–20 Å resolution through a 45.5" circular aperture.

With our Nearby Field Galaxy Survey (NFGS), our goal is to significantly extend Kennicutt's work. We have obtained integrated and nuclear spectroscopy, and U, B, R surface photometry, for a sample of 196 galaxies in the nearby field. This sample includes galaxies of all morphological types and spans 8 magnitudes in luminosity. We include galaxies from a broad range of local galaxy densities, attempting to avoid a bias towards a particular environment. Our use of the term "field" corresponds to that of Koo & Kron (1992) and Ellis (1997). We use these observations to study the emission and absorption line strengths, metallicities, star formation rates and star formation histories, morphologies, structural param-

eters, and colors of the sample galaxies. These data can be used as an aid in understanding the spectra and imagery of galaxies at larger distances, and in measuring the changes in their properties over time.

In this first paper we describe the sample selection and present the surface photometry data. In subsequent papers we will present the spectrophotometric data, and present further analysis of the complete data set. The structure of this paper is as follows. Section 2 discusses the sample selection. In Section 3 we discuss the observing strategy, data reduction, calibration issues and an assessment of the data quality and errors. We present the primary data products in section 4. We conclude with a short discussion (section 5). Notes on individual objects in the sample are collected in appendix A, and the details of the adopted photometric calibration procedure are given in appendix B.

2. SAMPLE SELECTION

We selected galaxies from the first CfA redshift catalog (CfA I), which contains galaxies to a limiting blue photographic magnitude of $m_Z = 14.5$ (Huchra et al. 1983). This catalog has several virtues: (1) it is nearly complete within its selection limits, (2) it contains galaxies with a large range in absolute magnitude ($-22 \lesssim M_Z \lesssim -13$ for $H_0=100 \text{ km s}^{-1} \text{ Mpc}^{-1}$), and (3) all galaxies in the catalog have been morphologically classified. As the CfA I catalog is too large (~ 2400 galaxies) for a full spectroscopic and photometric survey, we have selected a subsample of ~ 200 galaxies as described below. Our goal was to select a sample of galaxies which spans the full range of galaxy properties in the CfA sample.

Because the FAST spectrograph (Fabricant et al. 1998) used to obtain the galaxy spectra for this survey has a maximum slit length of $\sim 3'$, we wished to minimize the number of galaxies larger than the slit length. We avoided a strict diameter limit that might introduce a bias against low surface brightness galaxies. Instead, we selected higher luminosity galaxies (generally the largest) at greater distances by imposing a lower limit on radial velocity that increases with luminosity. After applying a correction for the motion of the Milky Way with respect to the Local Group standard of rest, this cutoff is $V_{LG}(\text{km s}^{-1}) > 10^{-0.19-0.2M_Z}$. We take for the velocity with respect to the Local Group standard of rest: $V_{LG} = V_{helio} + 300 \cos(b) \sin(l)$. This approximates the result of Yahil et al. (1977). Here, we calculate galaxy distances directly from V_{LG} , assuming $H_0=100 \text{ km s}^{-1} \text{ Mpc}^{-1}$. No correction for infall towards the Virgo Cluster was applied at this stage.

In order to avoid a sampling bias favoring a cluster

population we also excluded galaxies in the direction of the Virgo Cluster with $V_{LG} < 2000 \text{ km s}^{-1}$ in the RA and DEC ranges given by Binggeli et al. (1985). A total of 1006 galaxies are left after our radial velocity and Virgo Cluster cuts, only a few of which are larger than $3'$.

Our goal was to reduce this number to ~ 200 galaxies with a distribution in M_Z that spans the full range in galaxy luminosities, and that fairly samples the changing mix of morphological types as a function of M_Z . To this end, the sample was sorted into 1 magnitude wide bins of M_Z and within each bin by morphological type. We then selected every N th galaxy in each bin, where N is the ratio between the total and desired number of galaxies in the bin (chosen to approximate the local galaxy luminosity function, e.g. Marzke et al. 1994). The total number of galaxies entering our statistical sample is 196. The median redshift in this sample is 0.01, and the maximum redshift is ~ 0.07 (A12195+7535).

The morphological types used in the selection were taken from Huchra et al. (1983). The types as used elsewhere in this paper are mainly from a later release of the CfA redshift survey and its extensions (Huchra et al. 1997) and from independent reclassifications by the authors, S. Kannappan and J.P. Huchra, using our CCD imagery. The main difference between the original and updated types is that the fraction of unclassified spirals and “peculiars” has been reduced, and that a few galaxies that were clearly mistyped have been reclassified. The reclassifications have not biased the sample, as they are redistributed fairly evenly over morphological type.

In table 1 we collect the global parameters of our sample as used in the sample selection. Column (1) lists the galaxy identifications as used throughout this paper, while columns (2) and (3) give the common names (NGC, IC, or IAU anonymous notation) and UGC catalog number (Nilson 1973), respectively. Columns (4) through (7) contain the equatorial and Galactic coordinates. The equatorial coordinates were remeasured from the Digital Sky Survey (DSS), reduced to B1950.0, and are accurate to $\sim 1''$. Columns (8) through (10) list the original numeric morphological types (Huchra et al. 1983) as used in the sample selection, and the numeric types and their translation on the Hubble sequence as adopted throughout the further analysis of the data. Columns (11) and (12) give the systemic velocities, both heliocentric and reduced to the Local Group standard of rest. Column (13) lists the absolute magnitude calculated from the blue photographic magnitude (CGCG, Zwicky et al. 1961–8) and the systemic velocity, assuming a simple uniform Hubble flow and $H_0=100 \text{ km s}^{-1} \text{ Mpc}^{-1}$. Columns (14) and (15) list the blue

TABLE 1
IDENTIFICATION AND GLOBAL PARAMETERS OF THE SAMPLE GALAXIES.

ID	Name	UGC	α_{1950}	δ_{1950}	l_{II}	b_{II}	T	T	type	cz	V_{LG}	M_Z	a	ϵ	PA	A_g	data	
(1)	(2)	#	from DSS	(°)	(°)	sel [†]	new	new	(km/s)	(km/s)	mag	'	(1 - $\frac{b}{a}$)	°	mag	(16)	(17)	(18)
(3)	(4)	(5)	(6)	(7)	(8)	(9)	(10)	(11)	(12)	(13)	(14)	(15)	(16)	(17)	(18)			
1	A00113+3037	130	00 11 21.0	+30 36 18.3	113.518	-31.302	-6	-6	cE	4735	4858	-19.28	0.45	0.222	160	0.19	inubr	
2	A00289+0556	313	00 28 51.3	+05 55 50.1	113.942	-56.316	7	7	Sd	2055	2093	-17.42	1.40	0.429	10	0.17	inubr	
3	NGC 193	408	00 36 44.1	+03 03 23.7	116.977	-59.400	-3	-3	S0-	4340	4317	-18.95	1.70	0.059	55	0.07	inubr	
4	A00389-0159	439	00 38 48.1	-01 59 24.1	117.078	-64.473	1	1	Sa	5302	5243	-19.27	1.20	0.000	170	0.07	inubr	
5	A00442+3224	484	00 44 14.0	+32 24 08.9	121.836	-30.187	3	3	Sb	4859	4971	-19.43	2.80	0.714	25	0.20	inubr	
6	A00510+1225	545	00 50 57.8	+12 25 20.4	123.749	-50.175	-6	5	Sc	18116	18276	-22.31	0.60	0.167	—	0.20	inubr	
7	NGC 315	597	00 55 05.7	+30 04 57.7	124.563	-32.499	0	-5	E	4956	5050	-21.06	3.00	0.167	40	0.28	inubr	
8	A00570+1504	615	00 57 01.8	+15 03 42.0	125.870	-47.494	2	2	Sab	5517	5528	-19.57	1.00	0.500	23	0.16	inubr	
9	(A01047+1625)	685	01 04 43.0	+16 25 02.7	128.431	-46.017	10	10	Im	158	305	-13.03	1.90	0.316	120	0.11	inubr	
10	NGC 382	688	01 04 38.2	+32 08 13.7	126.836	-30.347	-7	-5	E	5228	5325	-19.48	0.25	0.000	—	0.19	inubr	
11	IC 1639	750	01 09 13.1	-00 55 46.4	134.223	-63.089	-6	-6	cE	5395	5321	-19.50	0.90	0.111	100	0.12	inubr	
12	A01123-0046	793	01 12 15.2	-00 45 36.8	135.794	-62.783	-6	5	Sc	10184	10280	-20.56	0.70	0.357	87	0.07	inubr	
13	A01187-0048	892	01 18 43.1	-00 48 22.4	139.243	-62.468	1	1	Sa	5240	5164	-19.13	2.10	0.000	125	0.13	inubr	
14	NGC 516	946	01 21 30.3	+09 17 26.9	136.240	-52.474	-2	-2	S0	2432	2445	-17.74	1.50	0.667	44	0.12	inubr	
15	A01300+1804	1104	01 30 00.3	+18 03 38.7	136.481	-43.466	10	10	Im	686	800	-15.31	1.20	0.333	5	0.13	inubr	
16	A01344+2838	1154	01 34 28.3	+28 08 09.3	134.893	-32.914	20	4	Sbc	7756	7801	-20.10	0.90	0.111	130	0.28	inubr	
17	A01346+0438	1155	01 34 31.3	+04 37 48.6	143.669	-56.137	15	4	Sbc	3158	3127	-18.06	0.90	0.222	166	0.05	inubr	
18	A01374+1539B	1176	01 37 28.8	+15 39 13.5	139.725	-45.370	10	10	Im	630	731	-15.02	5.00	0.200	30	0.16	br	
19	NGC 695	1315	01 48 27.6	+22 20 07.5	140.583	-38.231	15	5	Sc	9705	9855	-21.27	0.50	0.100	40	0.32	inubr	
20	(NGC 784)	1501	01 58 24.9	+28 35 42.5	140.905	-31.586	9	9	Sm	198	362	-15.68	6.80	0.735	0	0.23	ubr	
21	A02008+2350	1551	02 00 48.6	+23 50 06.7	143.373	-35.915	8	8	Sdm	2669	2734	-18.15	3.00	0.500	135	0.36	inubr	
22	IC 195	1555	02 01 02.0	+14 28 11.4	147.876	-44.632	-2	0	S0/a	3648	3646	-18.58	1.50	0.467	135	0.15	inubr	
23	IC 197	1564	02 01 29.6	+02 32 51.1	156.117	-55.334	4	4	Sbc	6332	6240	-19.73	1.00	0.500	55	0.05	inubr	
24	IC 1776	1579	02 02 37.8	+05 52 01.6	153.887	-52.273	5	5	Sc	3405	3363	-18.31	2.30	0.044	—	0.10	inubr	
25	A02056+1444	1630	02 05 41.5	+14 44 07.5	149.175	-43.942	20	3	Sb	4405	4392	-18.97	1.20	0.500	43	0.17	inubr	
26	NGC 825	1636	02 05 54.7	+06 05 13.9	154.894	-51.699	1	1	Sa	3403	3360	-18.21	2.50	0.560	53	0.12	inubr	
27	NGC 927	1908	02 23 55.1	+11 55 51.8	156.461	-44.432	5	5	Sc	8258	8191	-20.11	1.30	0.000	—	0.32	inubr	
28	A02257-0134	1945	02 25 39.8	-01 34 14.9	168.986	-55.318	20	8	Sdm	1762	1714	-16.87	2.40	0.625	12	0.04	inubr	
29	NGC 984	2059	02 31 51.6	+23 11 40.6	151.623	-33.641	5	1	Sa	4403	4425	-18.78	3.00	0.333	120	0.38	inubr	
30	NGC 1029	2149	02 36 54.7	+10 34 43.5	161.227	-43.889	0	0	S0/a	3635	3600	-18.74	1.60	0.688	70	0.33	inubr	
31	A02464+1807	2296	02 46 21.2	+18 07 39.8	158.307	-36.324	15	-6	cE	10010	10099	-21.92	0.90	0.000	—	0.34	ubr	
32	A02493-0122	2345	02 49 20.4	-01 22 34.7	176.063	-51.173	9	9	Sm	1508	1462	-16.71	4.50	0.222	—	0.17	inubr	
33	NGC 1298	2683	03 17 41.3	-02 17 38.5	184.276	-46.493	-5	-7	E	6528	6386	-19.87	1.20	0.083	70	0.20	inubr	
34	A03202-0205	2704	03 20 15.5	-02 06 01.4	184.637	-45.871	15	1	Sa	8227	8074	-20.27	1.00	0.000	—	0.13	inubr	
35	NGC 1552	3015	04 17 44.7	-00 48 43.5	194.160	-33.421	-2	-2	S0	4924	4797	-19.03	2.00	0.250	110	0.24	inubr	
36	NGC 2692	4675	08 53 22.1	+52 15 31.7	166.281	+40.132	1	1	Sa	3780	4033	-18.82	1.40	0.714	165	0.07	inubr	
37	A08567+5242	4713	08 56 44.3	+52 41 23.5	165.641	+40.592	3	3	Sb	9036	9233	-21.09	1.90	0.316	177	0.01	inubr	
38	A09045+3328	4787	09 04 30.8	+33 28 40.0	191.287	+41.809	8	8	Sdm	553	609	-14.23	2.30	0.783	6	0.03	inubr	
39	NGC 2780	4843	09 09 39.2	+35 07 54.5	189.253	+43.077	3	2	Sab	1951	2201	-17.21	1.00	0.300	150	0.02	inubr	
40	A09125+5303	4879	09 12 30.6	+53 03 04.1	164.662	+42.886	10	10	Im	600	819	-15.09	2.50	0.400	85	0.01	inubr	
41	NGC 2799	4909	09 14 17.6	+42 12 15.0	179.536	+44.323	9	9	Sm	1882	2165	-16.98	2.10	0.762	125	0.00	inubr	
42	NGC 2824	4933	09 16 06.9	+26 28 52.1	201.240	+42.921	-2	-2	S0	2760	2952	-17.84	1.00	0.400	160	0.07	inubr	
43	NGC 2844	4971	09 18 37.9	+40 21 53.1	182.117	+45.153	1	1	Sa	1486	1770	-17.25	1.90	0.526	13	0.00	inubr	
44	NGC 3011	5259	09 46 44.4	+32 27 18.3	194.246	+50.484	-2	0	S0/a	1517	1798	-16.64	0.90	0.111	52	0.01	inubr	
45	NGC 3009	5264	09 47 01.9	+44 31 45.0	175.323	+50.032	20	5	Sc	4666	4904	-18.85	0.80	0.125	—	0.01	inubr	
46	IC 2520	5335	09 53 28.6	+27 27 58.0	202.394	+51.265	15	15	..//Pec	1226	1478	-16.01	0.70	0.143	—	0.04	inubr	
47	A09557+4758	5354	09 55 42.1	+47 58 33.8	169.531	+50.736	20	9	Sm	1172	1498	-16.01	2.30	0.435	75	0.00	inubr	
48	NGC 3075	5360	09 56 13.7	+14 39 33.5	221.580	+47.958	5	5	Sc	3566	3714	-18.18	1.20	0.333	135	0.05	inubr	
49	A09579+0439	5378	09 57 55.6	+04 38 52.4	234.367	+43.385	3	3	Sb	4185	4270	-18.81	1.80	0.556	103	0.00	inubr	
50	NGC 3104	5414	10 00 56.4	+41 00 05.2	180.288	+53.105	10	10	Im	604	711	-14.70	3.60	0.361	35	0.05	inubr	
51	A10042+4716	5451	10 04 10.8	+47 15 03.3	170.003	+52.311	10	10	Im	571	724	-14.80	1.60	0.500	103	0.00	inubr	
52	NGC 3165	5512	10 10 55.6	+03 37 26.2	238.152	+45.447	10	10	Im	1317	1479	-15.78	1.60	0.500	177	0.01	inubr	
53	A10114+0716	5522	10 11 21.4	+07 16 20.2	233.886	+47.619	5	5	Sc	1228	1396	-15.74	3.00	0.400	145	0.00	inubr	
54	NGC 3179	5555	10 14 57.9	+41 21 52.8	178.895	+55.642	-2	-2	S0	7258	7467	-20.10	2.00	0.750	48	0.00	inubr	
55	A10171+3853	5577	10 17 07.4	+38 52 07.1	183.170	+56.483	15	9	Sm	2008	2328	-17.20	1.00	0.200	100	0.00	inubr	
56	NGC 3213	5590	10 18 33.4	+19 54 14.3	217.040	+54.882	4	4	Sbc	1412	1684	-16.28	1.10	0.273	133	0.06	inubr	
57	NGC 3264	5719	10 29 08.2	+56 20 27.6	153.937	+51.841	9	8	Sdm	929	1270	-15.72	3.50	0.571	177	0.00	inubr	
58	NGC 3279	5741	10 32 04.1	+11 27 22.1	232.621	+54.173	5	5	Sc	1422	1677	-16.44	2.80	0.875	152	0.12	inubr	
59	A10321+4649	5744	10 32 05.0	+46 49														

TABLE 1—Continued

ID	Name	UGC #	α_{1950} from DSS	δ_{1950}	l_{II} (°)	b_{II} (°)	T sel [†]	T new	type new	cz (km/s)	V_{LG} (km/s)	M_Z mag	a '	ϵ (1- $\frac{b}{a}$)	PA °	A_g mag	data	
(1)	(2)	(3)	(4)	(5)	(6)	(7)	(8)	(9)	(10)	(11)	(12)	(13)	(14)	(15)	(16)	(17)	(18)	
72	NGC 3499	6115	11 00 11.9	+56 29	28.5	149.136	+55.049	15	0	S0/a	1559	1951	-16.78	0.80	0.125	—	0.00	inubr
73	NGC 3510	6126	11 01 00.4	+29 09	23.0	202.364	+66.211	9	7	Sd	704	670	-15.29	4.20	0.786	163	0.00	inubr
74	A11017+3828W	6132W	11 01 40.6	+38 28	43.7	179.831	+65.032	-5	15	BL Lac	8887	9101	-21.64	0.80	0.250	90	0.00	inubr
75	NGC 3522	6159	11 04 00.8	+20 21	25.0	223.672	+65.045	-7	-3	S0-	1254	1602	-16.14	1.20	0.417	117	0.00	inubr
76	A11040+5130	6162	11 04 01.2	+51 28	26.5	155.195	+58.872	5	5	Sc	2204	2574	-17.58	2.50	0.520	88	0.00	inubr
77	IC 673	6200	11 06 51.6	+00 10	23.8	256.744	+53.368	1	1	Sa	3851	3982	-18.33	2.00	0.600	165	0.10	inubr
78	A11068+4705	6201	11 06 53.9	+47 05	08.5	161.608	+61.952	15	-3	S0-	7497	7752	-20.09	0.70	0.286	110	0.00	inubr
79	A11072+1302	6206	11 07 12.1	+13 02	32.0	239.032	+62.232	15	5	Sc	12743	12623	-21.31	0.90	0.444	18	0.00	inubr
80	NGC 3605	6295	11 14 08.6	+18 17	25.1	230.641	+66.378	-5	-3	S0-	686	551	-15.16	1.20	0.500	17	0.00	inubr
81	A11142+1804	6296	11 14 13.1	+18 04	19.8	231.145	+66.294	1	5	Sc	973	905	-15.42	1.30	0.692	166	0.00	inubr
82	NGC 3633	6351	11 17 51.7	+03 51	34.2	256.257	+57.958	1	1	Sa	2553	2771	-17.60	1.20	0.667	72	0.12	inubr
83	IC 692	6438	11 23 17.9	+10 15	45.3	249.231	+63.538	15	-5	E	1157	1501	-15.97	0.80	0.250	125	0.10	inubr
84	A11238+5401	6446	11 23 52.8	+54 01	19.7	147.561	+59.140	7	7	Sd	646	902	-14.81	4.10	0.366	10	0.00	ubr
85	A11310+3254	6545	11 31 05.4	+32 54	37.2	190.119	+72.312	15	3	Sb	2619	2953	-17.58	1.10	0.682	133	0.01	inubr
86	IC 708	6549	11 31 16.2	+49 20	19.2	152.024	+63.461	-7	7	E..	9438	9501	-20.69	1.40	0.357	175	0.00	inubr
87	A11332+3536	6570	11 33 10.9	+35 36	43.3	181.295	+71.917	0	-3	S0-	1598	1999	-16.52	1.20	0.500	123	0.04	inubr
88	A11336+5829	6575	11 33 40.9	+58 28	06.5	140.698	+56.274	5	5	Sc	1225	1632	-16.32	2.20	0.818	171	0.00	inubr
89	NGC 3795A	6616	11 36 37.1	+58 32	44.5	140.031	+56.402	6	6	Scd	1154	1559	-16.30	3.00	0.200	80	0.00	inubr
90	A11372+2012	6625	11 37 11.5	+20 12	38.8	232.798	+72.097	20	5	Sc	10964	10891	-20.99	0.80	0.125	55	0.00	inubr
91	NGC 3795	6629	11 37 22.8	+58 53	24.3	139.570	+56.152	20	5	Sc	1091	1491	-16.29	2.30	0.739	53	0.00	inubr
92	A11378+2840	6637	11 37 47.8	+28 39	03.9	204.276	+74.251	-2	-3	S0-	1821	2205	-16.76	0.90	0.556	72	0.00	inubr
93	A11392+1615	6655	11 39 15.2	+16 15	03.7	244.030	+70.384	15	-2	S0	786	619	-14.71	0.50	0.400	20	0.04	inubr
94	NGC 3846	6706	11 41 33.9	+55 18	45.4	141.998	+59.536	20	9	Sm	1396	1810	-16.67	2.10	0.143	40	0.00	inubr
95	NGC 3850	6733	11 42 55.0	+56 09	51.0	140.847	+58.893	5	5	Sc	1166	1573	-16.11	2.20	0.546	130	0.00	nubr
96	A11476+4220	6805	11 47 35.4	+42 21	10.0	158.913	+70.515	15	-2	S0	1033	1418	-15.94	0.35	0.286	105	0.00	inubr
97	NGC 3913	6813	11 48 00.5	+55 37	55.0	140.113	+59.700	7	7	Sd	953	1337	-15.91	3.00	0.067	165	0.00	nubr
98	IC746	6898	11 53 00.6	+26 10	04.1	215.437	+77.450	20	3	Sb	5027	5274	-18.99	1.30	0.731	169	0.00	inubr
99	A11531+0132	6903	11 53 03.1	+01 30	55.4	273.260	+60.852	5	5	Sc	1894	2187	-17.11	2.50	0.120	150	0.01	nubr
100	NGC 3978	6910	11 53 33.9	+60 48	02.6	134.848	+55.309	4	4	Sbc	9978	10099	-21.82	1.70	0.059	90	0.00	inubr
101	A11547+4933	6930	11 54 42.2	+49 33	41.7	144.546	+65.511	5	5	Sc	776	1076	-15.44	4.50	0.044	—	0.06	nubr
102	A11547+5813	6931	11 54 49.5	+58 12	30.4	136.375	+57.766	15	9	Sm	1175	1588	-16.04	1.70	0.353	80	0.00	inubr
103	NGC 4034	7006	11 58 55.9	+69 36	09.0	129.380	+47.174	5	5	Sc	2384	2779	-17.53	1.80	0.278	5	0.05	inubr
104	A11592+6237	7009	11 59 10.3	+62 36	21.1	132.686	+53.849	10	10	Im	1120	1533	-15.98	1.70	0.706	175	0.00	inubr
105	A12001+6439	7020A	12 00 04.1	+64 39	17.3	131.460	+51.936	-2	-2	S0	1447	1867	-16.70	1.20	0.500	100	0.02	inubr
106	NGC 4117	7112	12 05 14.1	+43 24	16.7	149.074	+71.716	-2	-2	S0	958	1332	-15.71	2.50	0.640	18	0.00	inubr
107	NGC 4120	7121	12 06 03.0	+69 49	19.4	128.420	+47.124	20	5	Sc	2251	2651	-17.81	1.80	0.778	166	0.03	inubr
108	A12064+4201	7129	12 06 23.2	+42 01	09.0	151.001	+72.991	2	2	Sab	927	1284	-15.63	1.30	0.385	75	0.00	inubr
109	NGC 4141	7147	12 07 17.9	+59 07	38.3	132.941	+57.463	5	5	Sc	1980	2392	-17.11	1.40	0.357	75	0.00	inubr
110	NGC 4159	7174	12 08 31.1	+76 24	14.1	126.126	+40.750	20	8	Sdm	1761	2169	-17.14	1.50	0.600	35	0.16	inubr
111	NGC 4204	7261	12 12 42.0	+20 56	13.7	249.038	+79.503	8	8	Sdm	861	707	-15.24	4.70	0.000	140	0.07	ubr
112	NGC 4238	7308	12 14 31.3	+63 41	16.5	129.380	+53.284	5	5	Sc	2771	3159	-18.12	1.80	0.750	36	0.03	inubr
113	NGC 4248	7335	12 15 21.6	+47 41	13.8	138.709	+68.676	0	8	Sdm	484	601	-14.83	3.20	0.594	108	0.00	inubr
114	A12167+4938	7358	12 16 44.6	+49 37	54.9	136.403	+66.922	5	5	Sc	3639	3992	-18.55	1.70	0.706	37	0.00	inubr
115	NGC 4272	7378	12 17 17.1	+30 36	59.4	186.227	+82.359	-5	-3	S0-	8453	8690	-20.43	1.00	0.100	—	0.07	nubr
116	NGC 4288	7399	12 18 10.3	+46 34	10.5	138.554	+69.891	9	9	Sm	532	653	-15.29	3.00	0.400	130	0.00	inubr
117	NGC 4308	7426	12 19 26.6	+30 21	05.2	186.726	+82.890	-5	-2	S0	641	590	-14.72	0.80	0.125	—	0.07	inubr
118	A12195+3222	7428	12 19 32.7	+32 22	19.9	173.298	+81.912	10	8	Sdm	1193	1648	-16.09	1.30	0.077	—	0.02	nubr
119	A12195+7353	7429	12 19 33.4	+75 35	16.4	125.447	+41.672	-6	-6	cE	21239	21422	-22.15	0.42	0.048	0	0.06	inubr
120	A12263+4331	7608	12 26 19.1	+43 30	10.2	137.407	+73.259	10	10	Im	535	622	-14.47	4.00	0.125	63	0.00	ubr
121	A12295+4007	7678	12 29 34.2	+40 06	30.6	139.315	+76.671	20	7	Sd	685	785	-15.42	1.60	0.375	88	0.00	inubr
122	A12300+4259	7690	12 30 01.5	+42 58	53.2	135.641	+73.951	10	8	Sdm	540	625	-15.18	2.30	0.217	20	0.00	inubr
123	A12304+3754	7699	12 30 21.5	+37 53	51.7	142.269	+78.797	6	7	Sd	503	526	-15.26	4.00	0.725	38	0.00	inubr
124	NGC 4509	7704	12 30 38.9	+32 22	02.1	160.567	+83.638	15	9	Sm	907	1204	-15.71	1.00	0.400	32	0.02	inubr
125	A12331+7230	7761	12 33 10.2	+72 30	25.6	124.677	+44.841	3	3	Sb	6959	7283	-19.97	0.70	0.286	100	0.04	inubr
126	A12446+5155	7950	12 44 39.4	+51 53	13.4	124.616	+65.499	10	10	Im	502	694	-14.81	1.80	0.278	75	0.00	inubr
127	NGC 4758	8014	12 50 14.6	+16 07	11.5	304.526	+78.716	10	4	Sbc	1244	1734	-16.29	3.00	0.733	160	0.01	inubr
128	NGC 4795	8037	12 52 31.4	+08 20	11.8	305.667	+70.918	-6	1	Sa	2812	3103	-19.08	2.10	0.143	115	0.00	inubr
129	NGC 4807	8049	12 53 03.5	+27 47	33.2	56.822												

TABLE 1—Continued

ID	Name	UGC	α_{1950}	δ_{1950}	l_{II}	b_{II}	T	T	type	cz	V_{LG}	M_Z	a'	ϵ	PA	A_g	data
(1)	(2)	#	from DSS	(°)	(°)	sel [†]	new	new	(km/s)	(km/s)	mag	(14)	(15)	(16)	(17)	(18)	
		(3)	(4)	(5)	(6)	(7)	(8)	(9)	(10)	(11)	(12)	(13)	(14)	(15)	(16)	(17)	(18)
143	A13422+3526	8693	13 42 15.2 +35 26 41.4	71.649	+76.101	20	4	Sbc	2502	2910	-17.55	1.30	0.692	167	0.00	inubr	
144	NGC 5338	8800	13 50 55.7 +05 27 12.6	339.653	+63.568	-2	-2	S0	777	722	-15.02	2.30	0.435	97	0.02	inubr	
145	NGC 5356	8831	13 52 27.7 +05 34 44.7	340.525	+63.469	3	3	Sb	1397	1787	-16.55	3.00	0.733	15	0.03	inubr	
146	A13550+4613	8876	13 54 57.9 +46 12 59.9	92.664	+67.115	0	0	S0/a	2133	2572	-17.46	0.90	0.722	27	0.00	inubr	
147	NGC 5407	8930	13 58 43.6 +39 23 50.8	77.083	+71.200	15	-2	S0	5431	5770	-19.21	1.40	0.286	100	0.00	inubr	
148	NGC 5425	8933	13 58 52.4 +48 41 01.9	95.270	+64.791	5	5	Sc	2062	2504	-17.40	1.90	0.763	127	0.04	inubr	
149	A14016+3559	8984	14 01 38.0 +35 58 52.2	66.632	+72.369	20	-2	S0	3829	4194	-18.76	1.30	0.769	35	0.00	inubr	
150	NGC 5470	9020	14 04 01.9 +06 16 01.4	346.552	+62.359	3	3	Sb	1023	1350	-15.48	2.60	0.846	63	0.04	nubr	
151	NGC 5491	9072A	14 08 27.7 +06 35 59.8	348.831	+61.926	20	5	Sc	5845	6075	-19.92	1.60	0.375	78	0.04	inubr	
152	NGC 5532	9137	14 14 26.4 +11 02 19.5	357.962	+64.112	-2	-2	S0	7367	7600	-21.03	1.60	0.000	148	0.00	inubr	
153	NGC 5541	9139	14 14 28.9 +39 49 13.3	73.541	+68.390	20	5	Sc	7698	8018	-21.06	0.90	0.222	4	0.00	inubr	
154	NGC 5596	9208	14 20 24.4 +37 20 56.4	66.131	+68.368	-2	-2	S0	3167	3559	-18.07	1.20	0.250	100	0.00	inubr	
155	NGC 5608	9219	14 21 18.8 +42 00 07.5	76.813	+66.192	10	9	Sm	662	966	-15.16	3.00	0.433	95	0.00	inubr	
156	A14305+1149	9356	14 30 28.3 +11 48 52.9	4.760	+61.575	20	5	Sc	2234	2598	-17.46	1.60	0.500	105	0.04	inubr	
157	NGC 5684	9402	14 33 47.5 +36 45 38.3	62.551	+66.010	-2	-2	S0	4082	4450	-18.91	1.90	0.158	105	0.00	inubr	
158	NGC 5762	9535	14 46 18.7 +12 39 52.1	10.617	+58.880	20	1	Sa	1788	2176	-17.00	2.00	0.250	140	0.03	inubr	
159	A14489+3547	9560	14 48 55.2 +35 46 37.4	58.761	+63.247	15	15	Pec	1215	1668	-16.12	0.80	0.688	65	0.00	inubr	
160	A14492+3545	9562	14 49 13.0 +35 44 50.1	58.674	+63.193	15	15	Pec	1306	1763	-16.56	1.10	0.000	30	0.00	inubr	
161	IC 1066	9573	14 50 31.8 +03 29 59.7	358.879	+52.425	20	2	Sab	1613	1963	-16.83	1.40	0.429	70	0.11	inubr	
162	A14594+4454	9660	14 59 22.8 +44 53 42.0	75.686	+58.725	15	5	Sc	626	976	-15.15	0.80	0.563	83	0.05	inubr	
163	A15016+1037	...	15 01 36.3 +10 37 55.9	11.209	+54.632	15	-6	cE	10921	10955	-21.20	0.20	0.000	—	0.07	inubr	
164	IC 1100	9729	15 05 22.5 +63 10 21.7	100.812	+47.943	20	6	Scd	6561	6918	-20.05	1.00	0.300	60	0.02	inubr	
165	NGC 5874	9736	15 06 27.2 +54 56 36.0	90.482	+52.907	4	4	Sbc	3128	3542	-18.50	2.60	0.346	53	0.01	inubr	
166	NGC 5875A	9741	15 07 03.1 +52 29 10.1	86.909	+54.147	15	5	Sc	2470	2903	-18.01	0.45	0.111	100	0.07	inubr	
167	NGC 5888	9771	15 11 17.4 +41 27 02.5	68.162	+57.768	3	3	Sb	8738	9067	-20.44	1.50	0.400	158	0.03	inubr	
168	IC 1124	9869	15 27 50.3 +23 48 32.3	36.378	+54.159	20	2	Sab	5242	5566	-19.14	0.90	0.556	80	0.17	inubr	
169	NGC 5940	9876	15 28 51.4 +07 37 37.9	12.996	+47.351	2	2	Sab	10144	10190	-20.74	0.80	0.000	—	0.10	inubr	
170	A15314+6744	9896	15 31 21.1 +67 43 27.5	103.308	+42.955	5	5	Sc	6461	6818	-19.72	1.60	0.250	10	0.06	in br	
171	NGC 5993	10007	15 42 42.4 +41 16 37.0	65.923	+52.014	3	3	Sb	9578	9747	-21.04	1.20	0.250	140	0.06	inubr	
172	IC 1141	10051	15 47 25.6 +12 33 01.0	22.512	+45.805	15	0	S0/a	4458	4757	-18.78	0.50	0.100	95	0.11	inubr	
173	IC 1144	10069	15 49 41.5 +43 33 59.8	69.250	+50.414	-3	0	S0/a	12096	12275	-21.05	0.70	0.286	100	0.04	inubr	
174	NGC 6007	10079	15 51 01.5 +12 06 23.4	22.509	+44.820	4	4	Sbc	10548	10629	-21.03	1.70	0.294	65	0.08	inubr	
175	A15523+1645	10086	15 52 24.5 +16 45 48.3	28.767	+46.454	-2	5	Sc	2191	2566	-17.30	0.70	0.714	177	0.07	inubr	
176	A15542+4800	10097	15 54 12.8 +48 00 42.4	75.757	+48.796	-2	-2	S0	5996	6361	-19.86	1.30	0.154	130	0.05	inubr	
177	NGC 6020	10100	15 54 58.1 +22 32 52.4	37.084	+47.814	-7	-7	E..	4397	4732	-18.77	1.40	0.286	140	0.12	inubr	
178	NGC 6123	10333	16 16 39.1 +62 03 36.3	93.481	+41.541	0	0	S0/a	3986	4381	-18.72	0.80	0.750	4	0.01	inubr	
179	NGC 6131	10356	16 20 07.7 +39 02 58.4	62.024	+44.988	5	5	Sc	5054	5419	-19.40	1.10	0.000	—	0.00	inubr	
180	NGC 6185	10444	16 31 28.1 +35 26 45.9	57.271	+42.480	9	1	Sa	10301	10487	-20.60	1.20	0.333	0	0.05	inubr	
181	NGC 7077	11755	21 27 27.5 +02 11 38.1	56.028	-33.234	-7	0	S0/a	1142	1323	-16.35	0.60	0.000	—	0.18	inubr	
182	NGC 7194	11888	22 01 04.5 +12 23 39.8	71.769	-33.080	-7	-7	E..	8139	8242	-20.12	1.30	0.308	20	0.27	inubr	
183	A22306+0750	12074	22 30 36.1 +07 50 23.6	74.425	-41.391	15	5	Sc	1995	2129	-17.52	0.60	0.333	145	0.33	inubr	
184	NGC 7328	12118	22 34 59.8 +10 16 17.7	77.618	-40.271	2	2	Sab	2827	2949	-18.12	2.10	0.667	88	0.23	inubr	
185	NGC 7360	12167	22 41 01.9 +03 53 21.7	73.386	-46.057	15	-5	E	4697	4756	-18.95	0.70	0.571	153	0.16	inubr	
186	A22426+0610	12178	22 42 37.2 +06 10 00.6	75.963	-44.620	15	8	Sdm	1925	2043	-17.44	3.30	0.485	10	0.15	inubr	
187	A22551+1931N	12265N	22 55 08.7 +19 31 22.1	89.474	-35.580	15	-2	S0	5682	5795	-18.56	0.20	0.250	90	0.15	inubr	
188	NGC 7436	12269	22 55 32.7 +25 52 56.6	93.384	-30.131	-7	-5	E..	7409	7537	-20.22	2.00	0.000	—	0.23	inubr	
189	NGC 7460	12312	22 59 09.8 +01 59 40.6	76.610	-50.471	3	3	Sb	3296	3352	-18.51	1.10	0.091	50	0.27	inubr	
190	NGC 7537	12442	23 12 01.8 +04 13 33.8	82.762	-50.661	4	4	Sbc	2648	2718	-18.13	2.10	0.762	79	0.20	inubr	
191	NGC 7548	12455	23 12 43.7 +25 00 33.8	96.951	-32.688	-2	-2	S0	7925	8035	-20.06	1.00	0.200	15	0.32	inubr	
192	A23176+1541	12519	23 17 32.3 +15 40 46.1	93.009	-41.547	20	7	Sd	4380	4472	-19.02	1.40	0.714	158	0.11	inubr	
193	NGC 7620	12520	23 17 37.2 +23 56 50.5	97.621	-34.122	6	6	Scd	9565	9811	-21.46	1.30	0.077	—	0.24	inubr	
194	A23264+1703	12620	23 26 23.9 +17 02 00.9	96.347	-41.264	-2	-2	S0	6849	6918	-20.05	1.40	0.143	—	0.11	inubr	
195	IC 1504	12734	23 38 46.2 +03 44 25.3	91.733	-54.551	3	3	Sb	6306	6307	-19.56	1.90	0.737	94	0.21	inubr	
196	NGC 7752	12779	23 44 27.1 +29 10 52.9	106.493	-31.346	0	7	Sd,pec	4902	5034	-19.26	0.45	0.556	113	0.20	inubr	
197	A23514+2813	12835	23 51 24.1 +28 12 52.0	107.907	-32.696	-7	-5	E	6946	7051	-19.88	1.10	0.273	0	0.16	inubr	
198	A23542+1633	12856	23 54 11.8 +16 32 09.3	104.568	-44.099	10	10	Im	1788	1908	-17.00	2.60	0.654	12	0.05	inubr	

[†] Unclassified spirals (S...?) are indicated by numeric type 20.

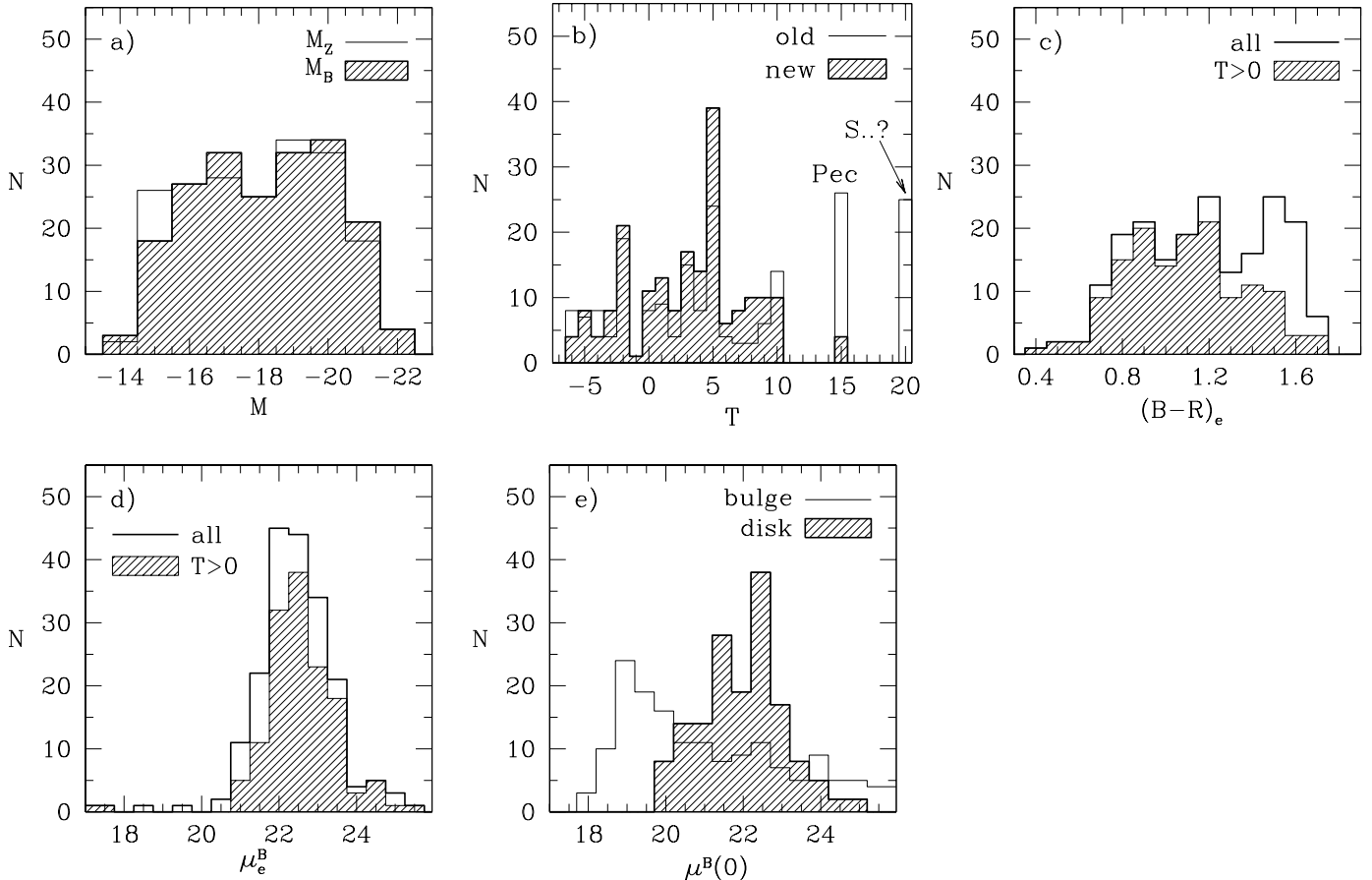


FIG. 1 — Overview of the global properties of the selected galaxy sample. We present the number distributions as a function of a) absolute Zwicky (open) and B (shaded) magnitudes; b) galaxy type, for the original type used in the selection of the sample (open) and for the types adopted in the present analysis (shaded). Note that here and in the following figures we place the unclassified early type galaxies at $T=-4$, as this bin is empty (we have no cD galaxies in our sample) and the proper placement at $T=-7$ seems awkward with respect to the compact ellipticals at $T=-6$; c) effective color $(B-R)_e$, measured within the effective radius in B . d) the surface brightness at the effective radius in B . In panels c) and d) the open histograms represent the selected sample, and the shaded histograms the subsample of galaxies later than S0/a; e) the face-on (extrapolated) central surface brightness of disks and spheroidal/elliptical components.

major axis diameters, a , and the ellipticities, $\epsilon = 1 - b/a$, derived from the minor and major axis ratio as listed in the UGC catalog. Column (16) gives the position angles of the major axis, measured from North through East, as given in the UGC. These position angles and the ellipticities in column (15) were used (section 3.2) to obtain radial intensity profiles. Column (17) gives the B -filter Galactic foreground extinction as estimated from the HI maps of Burstein & Heiles (1984) as given in the RC3 (de Vaucouleurs et al. 1991). The final column lists the available data, where abbreviations “i”, “n”, “u”, “b”, and “r” are used for integrated and nuclear spectra, and U , B , and R surface photometry, respectively. Italic font is used where no photometric exposures are available in U , B , or R ; bold-face font where the only observation was a short photometric “snapshot” exposure (see section 3.1).

To efficiently use the available telescope time, several more galaxies were included in our observations. The data for two of these, A01047+1625 and NGC 784, both very late type and very nearby, are presented in this paper as well, but are not part of the statistical sample. In table 1 these galaxies are shown with parentheses.

In figure 1 we give an overview of the main sample properties, comparing the selection properties with the observed magnitudes, colors and types. In figures 1a-d we plot for the 196 sample galaxies the number distributions of absolute magnitude (M_B and M_Z), morphological type (as selected and as reclassified), effective color $(B-R)_e$, measured within the effective radius r_e^B in B , and surface brightness in B at that effective radius.

We prefer the surface brightness measured at the effective radius over the (extrapolated) central surface

brightness, because (1) it can be measured for any light distribution (we need not a priori adopt a model for the light distribution, which might introduce artificial differences between galaxies of different morphological type), (2) the measurement is relatively robust, (3) no extrapolation is involved, and (4) it can be readily compared with results from numerical galaxy simulations. However, to facilitate comparison with data in the literature, we also fit the face-on (extrapolated) central disk surface brightness and exponential scale length for the galaxies with a disk component and, after subtraction of the disk, the face-on central surface brightness of bulge, or central condensation. The bulge and elliptical central surface brightnesses are uncertain as they depend critically on the light distribution in the inner few arcseconds of a galaxy. The result is plotted in figure 1e. We note that for a pure exponential disk the central surface brightness and the surface brightness at the effective radius are related by $\mu_e^B = \mu^B(0) + 1.0857(r_e^B/r_0^B) + 2.5 \log(1 - \epsilon)$, with r_0^B the exponential scale length.

MERITS AND LIMITATIONS OF THE SAMPLE

The final sample contains 196 nearby galaxies with a large range of absolute magnitudes ($-14 < M_B < -22$), extending about five magnitudes fainter than the characteristic local galaxy luminosity in B ($M_* \sim -19.2$, de Lapparent et al. 1989; $M_* \sim -18.8$, Marzke et al. 1994). By the selection process we assure sampling of the entire range of morphologies. Galaxies with several types of nuclear activity (Seyfert I and Seyfert II; BL Lac; nuclear star burst) are present in our sample. We also fairly sample a range of ~ 1.3 magnitude in effective $(B-R)_e$ color and the number distribution as a function of color is broad. (Our selection was unbiased towards color.) As expected, the early type galaxies are predominantly red while the spirals and later type galaxies cover a large range in color. The distribution of observed surface brightness at the effective radius in B has a peak at $22.0 \text{ mag arcsec}^{-2}$, a mean of $22.4 \text{ mag arcsec}^{-2}$, and a FWHM of $1.7 \text{ mag arcsec}^{-2}$. The tails of the distribution, however, extend over almost $10 \text{ mag arcsec}^{-2}$. The early type galaxies tend to be brighter at the effective radius than the late type galaxies. The distribution of face-on central disk surface brightness peaks at $\sim 22.5 \text{ mag arcsec}^{-2}$, has a mean of $22.0 \text{ mag arcsec}^{-2}$, and a FWHM of $2.6 \text{ mag arcsec}^{-2}$.

The sample contains several examples of low surface brightness (LSB) galaxies and galaxies containing LSB disks, the most extreme of which are A01374-

+1539B, A12263+4331 and A11238+5401 (but see also A10114+0716 and IC 673 for examples of LSBs with bulges). Although this sample, as most magnitude limited samples, is deficient in LSBs (Sprayberry et al. 1995; McGaugh, Schombert & Bothun 1995) *we do not omit this part of the galaxy population*.

We do not have any examples of the very brightest end of the cluster luminosity function, represented by the brightest cluster galaxies, in our final sample. These systems are very rare, however, in terms of their number frequency averaged over the entire field, and in terms of luminosity density. We also lack examples of galaxies at the very faintest end of the luminosity function (at $M_B > -14$), due to the negligible sample volume of the CfA I catalog at these faint absolute magnitudes. With few caveats, our sample is a faithful representation of the local field galaxy population.

3. OBSERVATIONS, REDUCTION AND CALIBRATION

3.1. Observations

The photometric observations reported here were made with CCD cameras at the F.L. Whipple Observatory's 1.2 m telescope¹. The data were obtained during 50 dark nights between 1994 March and 1997 March. We used both front-side and thinned back-side illuminated versions of Loral CCDs with 2048×2048 , $15 \mu\text{m}$ pixels. This yields a scale of $\sim 0.32''$ per pixel, although we usually binned the images 2 by 2. The images cover a region $\sim 11'$ square. For both CCDs the readout noise was $\sim 8 \text{ e}^-$ RMS.

We obtained B and R images with the front-side illuminated CCD, typically integrating 2×900 seconds in B and 2×450 seconds in R . Beginning in 1995 October, the back-side illuminated CCD camera was commissioned, allowing U exposures. We typically integrated 900 seconds in U , 2×450 seconds in B and 2×180 seconds in R with this CCD.

The U and B filters closely follow the Johnson (1955) system, while the R filter follows the Cousins (1976) system. The B filter has a small leak at 5600\AA that contributes $\sim 0.5\%$ to the total light for a flat spectrum source. On photometric nights, we observed several Landolt (1992) standard star fields at low and high airmass for photometric calibration. We obtained short and long exposures to allow the use of standard stars at a wide range of magnitudes and to check the CCD linearity. At least one standard star field was followed throughout most of the night. On photometric nights, we typically obtained short galaxy exposures to calibrate the non-photometric observations. The diameters of stellar images on our

¹The F.L. Whipple Observatory is operated by the Smithsonian Astrophysical Observatory, and is located on Mt. Hopkins in Arizona.

frames are typically $1.5''$ to $2.0''$ FWHM.

3.2. Data reduction

The data were reduced within the IRAF environment using a custom reduction pipeline that follows standard reduction techniques. The sequence of steps is: (1) interpolation over bad columns, dead and hot pixels, (2) bias subtraction using the median of the bias frames, followed by removal of the mean pixel value in the overscan region, (3) dark current subtraction using a median of the dark exposures, (4) subtraction of scattered light from a field flattening lens (October 1995 data only), and (5) flat fielding, correcting for the pixel-to-pixel variations with dome flats and for the illumination variations with twilight flats.

Prior to flat fielding, the consistency of the flats from night to night over each run was checked. The field flattener/dewar window was cleaned just before the observing run and then left undisturbed. The flat fields of separate nights correlate very well (frame to frame deviations less than 0.2%), allowing us to construct a single flat field for each filter for an entire run.

Following flat fielding, the images without bright stars are flat to better than 0.8% overall, improving to better than 0.5% in the cropped central $5.3'$ square portion of the CCD used for photometric analysis of all but the most extended galaxies. Even in the cropped images the field of view is large enough for accurate determination of the sky level.

Ellipses were fit to all galaxy images to obtain radial intensity profiles using the procedures described in Franz et al. (1989) and Jørgensen et al. (1992), and references therein. Regions containing CCD defects, cosmic ray events, stars, and background or companion galaxies were excluded from the fit. The width of the fitted elliptical annuli grows by a factor 1.1 in each radial step. This maintains a nearly constant signal-to-noise-ratio in the azimuthally averaged intensities by compensating for the decline in surface brightness with radius. The fits were continued to the radius where only 60% of the elliptical annulus falls inside the image.

We first fit the position of the galaxy center, fixing the position angle and ellipticity at the UGC values (Nilson 1973), listed in table 1. Then, with the center fixed to the fitted position, the ellipticity and position angles were fitted. In each case where the fit converged, the ellipticity and position angle in the outer parts of the galaxies matched the UGC values within the errors (see also de Jong and van der Kruit (1994)), independent of the filter used. We therefore adopted the UGC ellipticities and position angles with two exceptions: A12446+5155 has a position angle of 75

rather than 5° , and A11336+5829 has a position angle of 171 (or -9) rather than 9° . If the UGC omits a position angle for a round, very disturbed, or very compact system, we use a position angle of 90° . The final radial intensity profile was then fitted with the galaxy center, ellipticity, and position angle fixed at all radii.

Our goal is to obtain accurate photometry and internally consistent colors and surface brightness profiles, not to investigate the details of the light distribution. Ellipses will fail to adequately represent the isophote shapes of some of the galaxies in the sample, including barred galaxies and many late type galaxies. In addition, many late type galaxies have ellipticities and position angles that vary with radius, and in some cases the isophote centers wander.

The non-photometric data were calibrated with the help of the short calibration exposures obtained during photometric conditions. In a few cases, no photometric image was available, and we averaged the photometric scaling for the bracketing images if both agreed to better than $\sim 30\%$. These exceptions have been clearly marked in the figures and data tables presenting our surface brightness profiles and measurements (section 4).

The sky value was determined from the mean of the intensities of the 5 outermost annuli. These annuli extend to the edge of the images and contain many thousands of pixels. The variance in the sky level is dominated by systematic errors, which we estimate from the peak-to-peak variation in the background level over the images, excluding linear gradients. The systematic errors in the sky level are typically 0.5%, except where bright neighbouring galaxies or stars are present.

3.3. Calibration

For each flux standard star we measured instrumental magnitudes in a $14''$ diameter circular aperture for conformity with Landolt's (1992) photo-electric flux measurements. For each filter on each photometric night we used an interactive fitting procedure to find the photometric zeropoint, atmospheric extinction coefficient and color term coefficient. A night was declared non-photometric if: (1) we detected clouds or brightness fluctuations of the guide star, or (2) the RMS scatter in the photometric fit to the standard stars exceeded 0.035, 0.028, and 0.025 mag in U , B , and R respectively, or (3) the scatter in the photometric fit was time varying. Table 2 gives typical photometric constants for each filter and both CCD detectors. The sigmas in this table denote the spread (not the errors) of the fitted coefficients in almost 2 years of standard star data for each CCD.

TABLE 2

AVERAGE PHOTOMETRIC CONSTANTS FLWO 1994–1997

filter	CCD	zeropoint		extinction coeff.		color term coeff.		color
		p_z	σ_{pz}	p_e	σ_{pe}	p_c	σ_{pc}	
U	thick	19.97	0.08	0.482	0.039	-0.049	0.007	$U - R$
U	thin	21.76	0.06	0.482	0.039	-0.046	0.006	$U - R$
B	thick	21.61	0.09	0.252	0.022	-0.067	0.010	$B - R$
B	thin	23.24	0.05	0.252	0.022	-0.024	0.008	$B - R$
V^a	thick	21.93	—	0.112	—	+0.008	—	$B - V$
V^a	thin	23.04	0.08	0.151	0.034	+0.043	0.015	$B - V$
R	thick	22.10	0.11	0.115	0.020	+0.035	0.005	$B - R$
R	thin	23.14	0.06	0.115	0.020	+0.027	0.007	$B - R$
I^a	thin	22.92	0.05	0.053	0.023	-0.085	0.012	$R - I$

^a V and I filter standards were observed for co-scheduled monitoring programs.

The radial intensity profiles were then photometrically calibrated, solving simultaneously the calibration equations for B and R , or U and R , using $(B-R)$ and $(U-R)$ color terms, respectively. The details of this procedure are found in appendix B.

Finally, the calibrated surface brightness profiles were combined if multiple exposures were available. Because the repeated exposures were frequently obtained on different nights and even on different observing runs, the scatter in the individual profiles allows us to estimate the photometric errors. Where the variance of the calibrated profiles exceeds the formal photometric errors (see appendix B), we adopt this larger variance as our photometric error. In most cases this applies only to the inner few arcseconds of the profiles, where seeing changes (1.2–2.5") cause up to ~ 0.2 mag arcsec $^{-2}$ variations between individual profiles. We conclude that the shapes of the derived surface brightness profiles are reliable.

The radial surface brightness profiles were corrected for Galactic extinction, estimated from the HI maps of Burstein & Heiles (1984) and using extinction ratios $A_R/A_B = 0.588$ and $A_U/A_B = 1.156$ (Rieke & Lebofsky 1985) to derive the corrections in R and U . No corrections for cosmological effects (dimming and k -correction) were applied.

The profiles were used to measure isophotal and fractional magnitudes, and corresponding radii and colors (section 4.1).

For our photometric analysis it sufficed to match the individual surface brightness profiles of a galaxy. The individual images were not shifted to a common center, nor rebinned to a common position angle and pixel scale. Stars were not removed from the images. Also, we did not remove residual linear gradients in the background as they dropped out in the fitting of the ellipses. Although, in principle, these data are suitable for two-dimensional bulge/bar/disk deconvolutions and other detailed studies of the light distribution, at present the data are not in an easily

distributable format.

3.4. Total magnitudes: extrapolation to infinity

Following Han (1992) we extrapolated the radial surface brightness profiles to infinity to obtain total magnitudes, under the assumption that the light at large radii can be approximated by an exponential disk. Exponentials were fit to the outer parts of each radial surface profile over a 2.172 magnitude interval ending 0.3 mag arcsec $^{-2}$ above the 1 σ limiting isophote. For a purely exponential profile this surface brightness interval corresponds to exactly two exponential scale lengths. Our profiles are sufficiently deep that the details of the light fall off do not seriously affect the result. We might underestimate the luminosity of an $R^{1/4}$ profile elliptical by ~ 0.1 mag with this procedure. For disk galaxies the extrapolation procedure should work very well unless the disk is truncated near the outer fit interval. However, we found no convincing evidence for disk truncation in our sample. Furthermore, the galaxies requiring the largest corrections from isophotal to total magnitude follow an exponential profile to the faintest regions sampled in our data. The average limiting isophotes for our data are $\mu_U=26.7$, $\mu_B=27.2$, and $\mu_R=26.1$, with a spread of ~ 0.7 mag arcsec $^{-2}$.

Absolute magnitudes were calculated using the total magnitudes and the galaxy recessional velocities with respect to the centroid of the Local Group, correcting for Virgo infall. We used the infall model of Kraan-Korteweg et al. (1984) which has the Local Group falling in Virgo at 220 km s $^{-1}$; no other corrections for peculiar motion were applied.

3.5. Evaluation of the data quality

INTERNAL CONSISTENCY AND ERROR ANALYSIS

For most galaxies, more than one long exposure per filter is available. To evaluate the internal accuracy of our photometry we compare total and isophotal magnitudes measured in the radial surface brightness profiles derived from the individual exposures. In the many cases where we compare data from before October 1995 with later observations, we compare measurements obtained with different cameras.

We find RMS differences between individual measurements of the total magnitude (expressed in magnitudes and in units of the error of measurement) of 0.05 mag ($0.86\sigma_U$), 0.03 mag ($0.72\sigma_B$) and 0.03 mag ($0.66\sigma_R$) in U , B and R , respectively. For the majority of the sample, however, individual measurements agree to better than the values quoted above; typical values would be 0.030, 0.013, and 0.012 mag in U , B and R . This result is consistent with the estimated accuracy based on the errors in the fitted zeropoints

“fig2.jpg”

A 600 dpi postscript version of this preprint, including all figures and the atlas of galaxy images and radial profiles, can be retrieved from URL <http://www.astro.rug.nl/~nfgs/>

FIG. 2 — Comparison of our surface brightness profiles and profiles published by other authors. The difference $\Delta\mu$ is in the sense (our profiles – literature profiles). Offsets in photometric zeropoint are indicated where applied. As an aid in distinguishing significant differences between profiles we plot 1σ deviations as thin vertical bars. Key to the abbreviations used: SB'99=Swaters and Balcells (1999), TVPHW'96=Tully et al. (1996), dJvdK'94=de Jong and van der Kruit (1994), PDDIC'90=Peletier et al. (1990), and vdK'87=van der Kruit (1987).

and in the photometric scaling of non-photometric exposures. The measured differences do not depend on galaxy color, morphological type, date of observation, absolute magnitude, nor on effective surface brightness.

A more demanding test of our photometry, however, is a comparison with surface photometry published by other authors.

COMPARISON WITH OTHER AUTHORS

Our sample has 16 galaxies in common with the dwarf galaxy sample of Swaters & Balcells (in prep.; hereafter SB99), most of which were observed by these authors in R only; they observed only two of the 16 in B . Rob Swaters kindly provided us with his surface brightness profiles, allowing us to evaluate the external accuracy of our photometry. The results are presented in figure 2. We find good agreement for all galaxies that were observed under photometric conditions in both studies. Where SB99 note that cirrus was present (Swaters 1998, private comm.), we are able to compare the shape of the two sets of profiles after applying an offset (see figure text). Where necessary, we correct the SB99 results to account for a different assumed ellipticity; this correction never exceeded $\sim 10\%$.

We have 6 galaxies in common with another recent study of galaxies in the Ursa Major cluster (Tully et al. 1996; hereafter TVPHW96). These authors present B, R, I and K data. Marc Verheijen kindly provided us with tables of the data plotted in TVPHW96. Here again the photometric zeropoints agree well. In the worst cases, the surface brightness profiles at very large radii deviate by a few tenths of a magnitude per square arcsecond. For A11547+4933 our photometry is not very deep, and the R profiles of SB99 and TVPHW96 seem to be of higher quality.

We also show comparisons for a small number of galaxies in common with Peletier et al. (1990, PDDIC90), de Jong & van der Kruit (1994, dJvdK94), and the earlier photographic work of van der Kruit (1987). Comparisons with Kent (1988) for NGC 2844 and Patterson & Thuan (1996, PT96) for A12263+4331, are not shown in figure 2, but are poor. We note that our R profile of A12263+4331 agrees well with SB99.

4. PHOTOMETRIC RESULTS

4.1. Data presentation

Here we describe our primary data products, galaxy images and radial profiles of surface brightness and color, and present our photometric measurements. For 198 galaxies, our atlas includes logarithmically scaled renditions of the B images, B surface brightness profiles, and plots of $(U-B)$ and $(B-R)$ colors

as a function of radius (figure 3). The galaxies have been sorted by morphological type, and within each type by blue luminosity.

The radial profiles are not corrected for seeing, and are not a faithful representation of the surface brightness at small radii less than a few arcseconds. In some cases the inner part of a surface brightness profile appears to flatten over a larger region than that affected by seeing. This extended flattening results from a bar, irregularly distributed central star formation, dust, or multiple nuclei. Notes on individual galaxies and their radial profiles are collected in Appendix A.

The photometric measurements are collected in table 3. Columns (1) through (3) list the galaxy identifications. Column (4) gives the distances in Mpc derived from the Virgocentric flow corrected velocities with respect to the centroid of the Local Group (column (12) of table 1), assuming $H_0=100 \text{ km s}^{-1} \text{ Mpc}^{-1}$. Columns (5) and (6) list the B apparent and absolute total magnitudes. In columns (7) and (8) we give the elliptical radii, r_{26}^B , at which the surface brightness has dropped to $\mu_B=26 \text{ mag arcsec}^{-2}$ and the corresponding isophotal magnitude, B_{26} . Columns (9) and (10) list the effective (i.e. half-light) elliptical radius in B , r_e^B , and the surface brightness, μ_e^B , at that radius. Columns (11) and (12) contain the effective $(U-B)$ and $(B-R)$ colors as measured within the effective radii in B . The final two columns list the color differences, $\Delta(U-B)_{25-75}$ and $\Delta(B-R)_{25-75}$, between the inner and outer parts of the galaxies, as defined below.

Several authors have investigated the Zwicky magnitude scale. Bothun & Cornell (1990) showed for a sample of 107 spiral galaxies with $m_Z \geq 14.0$ that, although Zwicky magnitudes are not isophotal magnitudes, the scatter around isophotal magnitudes varying from B_{22} to B_{27} is of the order of 0.3 mag. In the mean, m_Z corresponds to B_{26} with a scatter of 0.31 mag. In figure 4a we plot the isophotal magnitudes measured within the elliptical aperture corresponding to the $\mu_B=26 \text{ mag arcsec}^{-2}$ isophote versus the photographic Zwicky magnitudes. We find for our sample a similar correspondence between m_Z and B_{26} with observed RMSs of 0.30 mag for galaxies with $m_Z < 14$ and of 0.42 mag for $m_Z \geq 14$. Using total magnitudes instead of B_{26} (figure 4b) gives a nearly identical result. Figure 4c shows that there is a relation between the difference $(m_Z - B_{26})$ and B_{26} for $m_Z > 14$: Zwicky tends to overestimate the magnitude (i.e. underestimate the brightness) of the brighter galaxies and underestimate the magnitudes of the fainter ones. The dependence of the magnitude difference on galaxy type is weak, with a very large

*Atlas of images and radial profiles — pages 12 through 46
 (“fig3_01.jpg” through “fig3_35.jpg”)*

A 600 dpi postscript version of this preprint, including all figures and the atlas of galaxy images and radial profiles, can be retrieved from URL <http://www.astro.rug.nl/~nfgs/>

FIG. 3 — The atlas of images and radial profiles. Greyscale renditions of a B filter image and the radial dependence of the surface brightness in U, B, R (top panel) and corresponding colors (bottom panel) are presented for each of the observed galaxies. The galaxies have been ordered according to their morphological type and per type according to their absolute B magnitude (both given in the images). North is up and East is to the left. The original CCD images were much larger than the portion centered on the galaxies presented here. The image scale is given by a scale bar of the indicated number of kpc (assuming $H_0=100 \text{ km s}^{-1} \text{ Mpc}^{-1}$), and is given on the top axis of the radial profile plots for reference. On the ordinate of the radial profile plots r denotes the elliptical radius in arcseconds. The extrapolation of the surface brightness profiles beyond the limiting isophote (see text) is indicated by grey lines. The effective radius in B is indicated by a small vertical arrow. Shallow profiles (only short photometric exposures are available) are indicated by (s), truncated profiles (due to overlapping neighbours or bright stars close to a galaxy) are indicated by (t), and profiles with uncertain photometric zeropoints by (z) or (z!). The names of the two galaxies not part of the statistical sample are placed in parentheses.

Compact ellipticals (page 12) through Irregulars (page 46).

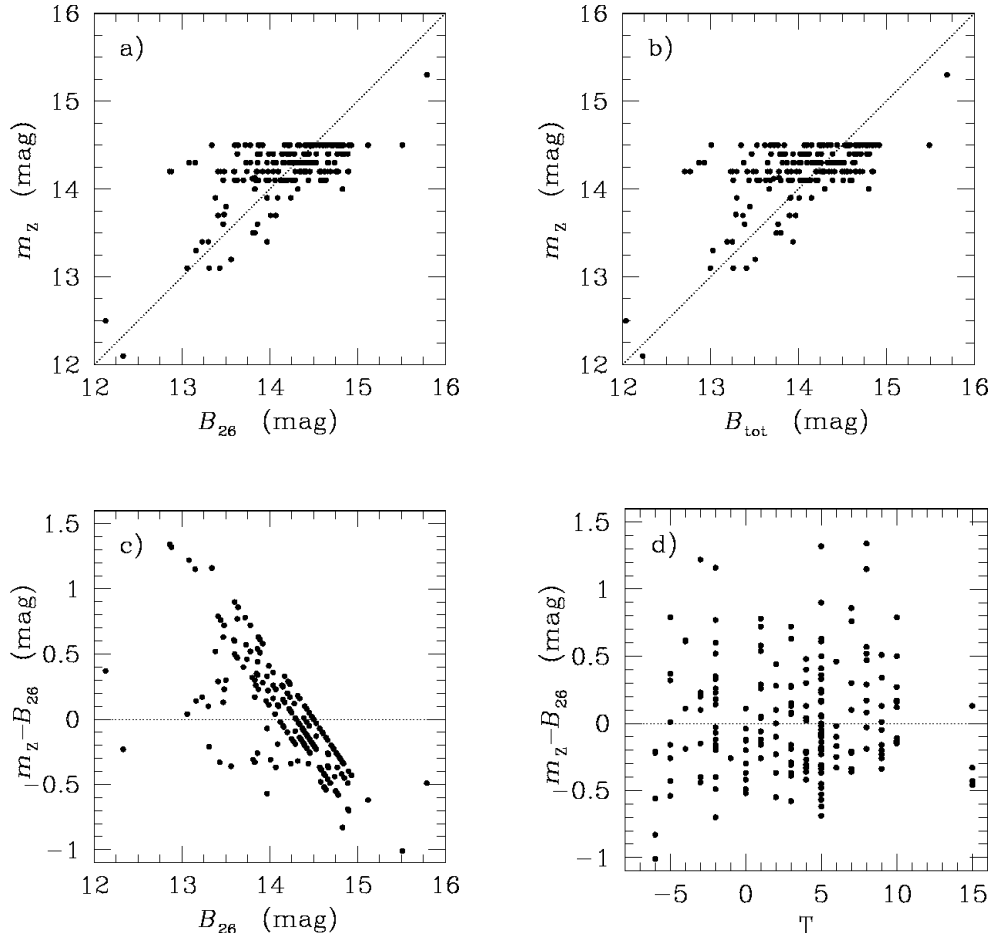


FIG. 4 — Comparison of photographic Zwicky magnitudes and a) B_{26} isophotal magnitudes, and b) total B magnitudes. For m_z brighter than 14 the observed RMS is 0.30 in both cases; for $m_z \geq 14$ the RMS is 0.42 and 0.45 mag for isophotal and total magnitudes, respectively. c) Difference $m_z - B_{26}$ as a function of B_{26} . For $m_z > 14$ this difference is correlated with isophotal magnitude. d) $m_z - B_{26}$ as a function of galaxy type. A weak trend of larger differences towards later galaxy type may be discerned, but the scatter on this trend is large.

scatter: Zwicky magnitudes for late type galaxies tend to be somewhat overestimated, while those for early type galaxies are underestimated. This dependence on morphological type was also inferred by Bothun & Cornell (1990) based on weak trends of ($m_z - B_{26}$) with a light concentration parameter and average surface brightness in their sample.

4.2. Properties of our sample

In Figure 5a we plot the distribution of total absolute B magnitudes as a function of numeric galaxy type. We show all galaxies, including active galaxies (starbursts or active galactic nuclei (AGN)). The range in luminosity and type is large (cf. figure 1), and galaxies of each type are distributed over a large range in absolute magnitude. However, the lack of intrinsically bright ($M_B \lesssim -19$) late type spirals and irregular systems ($T > 6$), and of low luminosity early and intermediate type spiral galaxies ($1 < T < 5$) is evident. This corresponds to the type–magnitude relation for spiral galaxies later than Sa found by other authors (see Sandage & Binggeli 1984, their figure 1).

Our sample does include a number of low luminosity early type S0 and elliptical systems. The BL Lac galaxy Mrk 421 and the Seyfert I galaxies are amongst the intrinsically brightest galaxies in our sample.

In figure 5b we plot the distribution of the effective ($B - R$) color (measured within the effective radius in B) as a function of galaxy type. The bulk of the galaxies become progressively bluer towards later types. This is not a new result, but the scatter on this trend is surprisingly small ($\sigma(B - R)_e = 0.19$ mag). Nonetheless, there are examples of very blue early-type and reddish late-type galaxies. The next panel shows that the blue early type galaxies tend to be low luminosity systems. If redshifts are available, color may be used to estimate a galaxy's broad type class (E,S,Irr) to a similar precision (~ 5 T types) as measures of galaxy asymmetry and concentration of the light (Abraham et al. 1996; see also Jansen et al. (in prep.) for an application of that method to our sample). This result is remarkable if not entirely new (de Vaucouleurs 1977; Tinsley 1980).

In figure 5c the distribution of effective galaxy colors is given as a function of absolute B magnitude. Luminous systems tend to be redder than fainter ones. This is a relationship well-established for early type galaxies (e.g. Sandage & Visvanathan 1978; Peletier et al. 1990; Ellis et al. 1997). The scatter in color for all galaxy types combined is larger ($\sigma(B-R)_e = 0.23$ mag) than that for the color-type relation. The scatter for the separate type classes E–S0, S0/a–Sab, Sb–Sc and Scd–Irr is 0.10, 0.15, 0.17 and 0.13 mag (median absolute deviation (MAD)), respectively. It is striking that ellipticals, S0's, and early type spiral galaxies occupy a different region in the plot than the late type spiral and irregular galaxies. The intermediate type spirals can be found mixed with both early and late type systems. The two distributions are offset from one another by ~ 0.4 mag in $(B-R)_e$ color, but there is a large overlap. This result persists if total colors are used or colors measured in the region between the radii containing 25% and 75% of the light in B .

Figure 5d is the color–color diagram of effective $(U-B)$ versus $(B-R)$ colors. The bulk of the normal galaxies follow a relation with only a small scatter (Tinsley 1980). The “abnormal” galaxies (harboring star bursts or an active nucleus, or interacting with another galaxy) show a much larger scatter (Larson & Tinsley 1978; Tinsley 1980). Again, we see that late and early type galaxies tend to occupy different regions in the plot, with early type galaxies located at redder colors. The relations followed by early and late type systems differ in slope, with the early type galaxies following a steeper slope. The dust extinction vector points nearly along the relation followed by the intermediate and late type spirals and irregular systems. Starburst galaxies tend to lie below and to the left of the main relation, i.e. at bluer $(U-B)$ colors for a given $(B-R)$ color.

In the following plots, figures 5e and f, we will plot only measurements for the 168 normal (non-AGN, non-starburst) galaxies in our sample with high quality photometry. Figure 5e shows the (trivial) relation, that larger galaxies are more luminous. We plot the logarithm of the effective radius in kpc as a function of absolute magnitude. As more strongly concentrated systems have smaller effective radii at a given absolute magnitude, we expect the early type galaxies and spirals with significant bulges to follow a relation offset from that followed by later type systems. Indeed, we find that galaxies fainter than $M_B \sim -19$ show a clear separation according to type. For the brightest systems, $M_B < -19$, this separation is not clear. Lower surface brightness galaxies lie above the mean relation for a given absolute magnitude and given type.

In figure 5f we plot the average R surface brightness within the effective radius, $\mu_{r \leq r_e}^R$, as a function of numeric galaxy type. The light distribution in early type galaxies is more concentrated (i.e. brighter in their inner parts) than that in later type galaxies. For spiral galaxies there is a strong trend towards fainter $\mu_{r \leq r_e}^R$ at later types, consistent with a decreasing contribution of bulges. There is no clear trend within the late type spirals and irregulars. A similar conclusion is reached if the average B surface brightness within the effective radius is used, but the trend is somewhat less pronounced.

We now explore the radial color gradient in our sample galaxies. We measure $(B-R)$ in the central region of the galaxy that contains 25% of the light, $(B-R)_{25}$, and in the region that contains the next 50% of the light, $(B-R)_{25-75}$. We define $\Delta(B-R)_{25-75}$ as the difference between these two measurements: $(B-R)_{25-75} - (B-R)_{25}$. $\Delta(U-B)_{25-75}$ is defined similarly. If $\Delta(B-R)_{25-75}$ is negative, the inner parts of the galaxy are redder than the outer parts.

Figure 6a is a plot of $\Delta(B-R)_{25-75}$ against galaxy type for the 168 “normal” galaxies. The median color difference values for each type have been connected by solid lines in this plot. The color difference between the inner and outer parts of a galaxy remains fairly constant for most of the early type galaxies ($T \leq 0$): the inner parts are on average 0.09 mag (with a range of ~ 0.15 mag) redder than the outer parts. Moving from S0/a to Sa, this difference becomes larger. The centers of spiral galaxies are redder by 0.18 mag, on average (with a range of ~ 0.30 mag), than their outer parts. The color differences decrease for late type spirals, reflecting the decreasing prominence of bulges and the more extended star formation. The inner parts of irregulars can be either bluer or redder than the outer parts. We will return to this issue below.

The bluing of galaxies at larger radii is not a new result (Sandage 1972; Persson, Frogel and Aaronson 1979; de Jong 1996). Recently, however, Tully et al. (1996) describe an absolute magnitude dependent behavior for galaxies in the Ursa Major cluster. These authors find that galaxies brighter than $M_B \sim -17$ become bluer with radius, and that fainter galaxies show the opposite behavior. We confirm this result (figure 6b), although the transition from a bluing trend with radius to a reddening trend may occur at a fainter limit. We find that *galaxies brighter than $M_B = -17$ are almost always redder in their inner parts, while galaxies fainter than $M_B \sim -17$ are equally likely to redden or blue with radius*. Panel c confirms that the majority of the galaxies that show

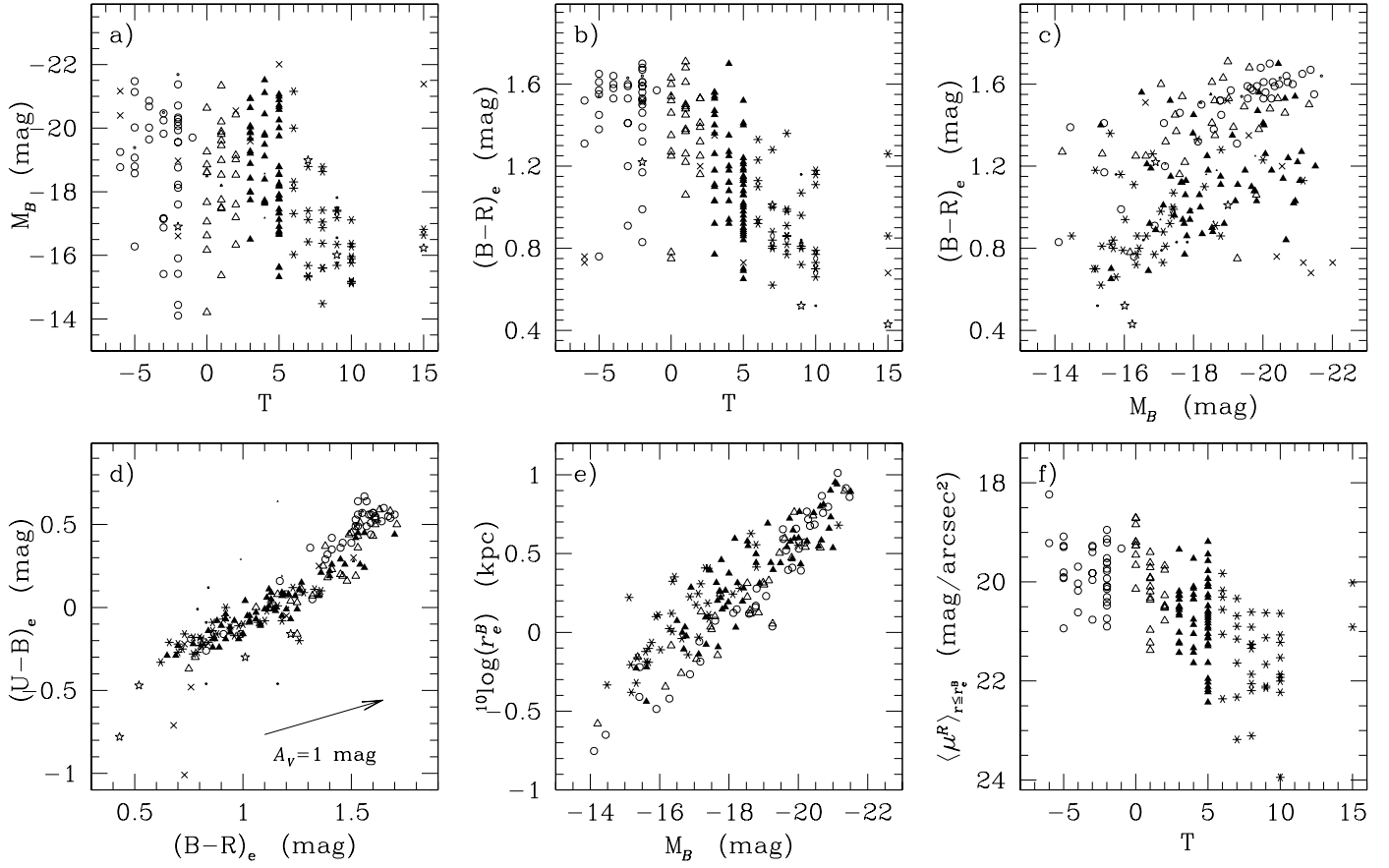


FIG. 5 — Photometric properties of the sample. Points are coded according to type as follows. For the normal galaxies, ellipticals and S0's ($T < 0$) are indicated by open circles, early type spirals ($0 \leq T < 3$) by open triangles, intermediate type spirals ($3 \leq T < 6$) by solid triangles and late type spirals and irregulars ($T \geq 6$) by asterisks. In the first four panels, galaxies with active nuclei (AGN) are indicated by crosses (Sy I, Sy II and BL Lac), starburst galaxies by open stars, and the few galaxies with uncertain photometric zeropoint by small symbols.

a) Total absolute B filter magnitudes as a function of numeric morphological type. Apart from the group of faint early type galaxies, the well-known trend of absolute magnitude with type — later type galaxies get progressively fainter — is evident. b) Effective $(B-R)$ colors as a function of type. Galaxies become progressively bluer towards later types. c) Effective $(B-R)$ colors versus total absolute B magnitude. Brighter galaxies tend to be redder. d) Color-color plot of effective $(U-B)$ versus $(B-R)$ colors. Apart from the active ones, the galaxies lie on a tight relation. Note that this is the first such plot for a sample so diverse in properties. The interstellar extinction vector is indicated. e) Effective radii in B versus total absolute B magnitude. Apart from the (trivial) relation between galaxy size and luminosity, we find a clear separation in type at a given magnitude for $M_B > -19$. Lower surface brightness galaxies lie above the mean relation for a given absolute magnitude and given type. f) Effective R -filter surface brightnesses measured within the effective radii in B as a function of type. Among the spiral galaxies a clear trend towards fainter $\langle \mu^R \rangle_{r \leq r_e^B}$ going to later types is visible.

a reddening with radius are blue, but that many redder systems shows this behaviour as well. Panel *d* identifies these systems as being physically smaller than average, while panel *a* shows that there is no preference towards morphological type. These results and inspection of the images in the atlas (e.g. IC 692 (E), A02257–0134 (Sdm), and A09125+5305 (Im)) suggest that star formation is the driving force in this reddening-with-radius trend; in large, luminous galaxies the star formation is stronger in the outer parts, while in smaller, fainter systems star formation may occur anywhere. In the latter case, a single HII-region can dominate the colors and its location may determine the radial color trend.

5. SUMMARY

We have completed a photometric and spectrophotometric survey of ~ 200 nearby galaxies of all morphological types and with a range of over 8 magnitudes in absolute B magnitude, with the goal of studying the variation in current star formation rates, star formation histories and metallicities as a function of galaxy type and luminosity. With this survey we extend the work of Kennicutt (1992) to lower luminosity systems. The U, B, R surface photometry will aid our interpretation of the spectrophotometry.

Here we have described the selection of our sample, the photometric observations and our data reduction techniques. We have presented our photometric data,

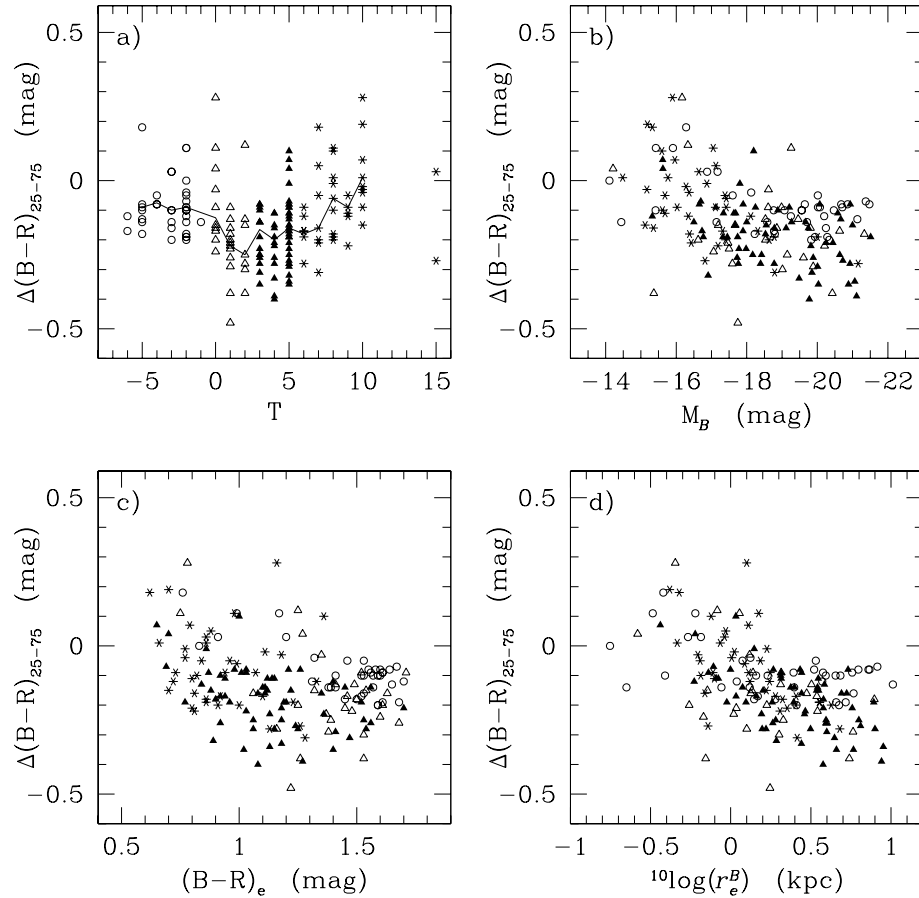


FIG. 6 — Color differences between inner and outer parts. a) The color difference $\Delta(B-R)_{25-75}$ (see text) as a function of type. The median color difference values have been connected by solid lines. The disappearance of a significant bulge going from early type spirals towards later types causes the strong trend for $T > 0$. b) $\Delta(B-R)_{25-75}$ as a function of total absolute B magnitude. Note that the galaxies fainter than $M_B \sim -16$ are equally likely to become redder with radius as they are to become bluer. c) $\Delta(B-R)_{25-75}$ as a function of effective $(B-R)$. Only a small majority of the galaxies showing a reddening trend with increasing radius is blue. d) $\Delta(B-R)_{25-75}$ as a function of effective radius in B . Galaxies showing a reddening trend with radius are intrinsically small systems.

including an atlas of galaxy images with radial profiles of surface brightness and $(U-B)$ and $(B-R)$ colors, and tables of photometric measurements. The spectrophotometry will be presented in a companion paper. Our surface photometry is consistent with previous published work in almost all cases where a comparison is possible, and the exceptions are described.

We find a strong trend of $(B-R)_e$ color with morphological type, with later type galaxies becoming progressively bluer. The observed scatter on this trend is 0.19 mag, which is smaller than the 0.24 mag scatter on the color-magnitude trend where intrinsically fainter systems tend to be bluer than brighter systems. Estimating a galaxy's broad type class (E,S,Irr) from its color can, therefore, be as accurate as estimates based on galaxy asymmetry and central concentration (Abraham et al. 1996). We find that color-magnitude relations are useful for early type systems and to a lesser degree for very late type sys-

tems, but not useful for intermediate type spirals. A color-color plot of $(U-B)_e$ versus $(B-R)_e$ shows a well defined relation with small scatter, considering the wide range in galaxy types, luminosities and colors in the sample.

Galaxies brighter than $M_B = -17$ are almost always reddest in their inner parts, but half the galaxies fainter than $M_B = -17$ are bluest in their inner parts. The total scatter in the radial color difference is large (~ 0.5 mag). Early and late type galaxies behave similarly and we conclude that low luminosity dwarf galaxies forming stars in their inner parts account for the reddening with radius. Tully et al. (1996) find that faint blue galaxies in the Ursa Major cluster behave similarly.

Both the average difference in color between the inner and outer parts of a galaxy and the range in color difference from galaxy to galaxy are smaller in early type galaxies than in spirals.

ACKNOWLEDGEMENTS

This work was supported by grants from the University of Groningen, the Leiden Kerkhoven-Bosscha Fund, the Netherlands Organisation for Scientific Research (NWO), and by the Smithsonian Institution. RAJ thanks the Harvard-Smithsonian Center for Astrophysics and the F.L. Whipple Observatory for hospitality during numerous visits, when all of the observations and part of this work was done. We thank C. Briceño, N.A. Grogin, K.K. McLeod, and T. Groner for giving us some of their observing time. We acknowledge comments made by the referee, Dr. G.D. Bothun, which helped to clarify some aspects of this paper.

REFERENCES

- Abraham, R. G., Tanvir, N. R., Santiago, B. X., Ellis, R. S., Glazebrook, K., & van den Bergh, S. 1996, MNRAS, 279, L47
- Binggeli, B., Sandage, A., & Tammann, G. A. 1985, AJ, 90, 1759
- Bothun, G. D., & Cornell, M. E. 1990, AJ, 99, 1004
- Burstein, D., & Heiles, C. 1984, ApJS, 54, 33.
- Cousins, A. W. J. 1976, MmRAS, 81, 25
- de Jong, R. S., & van der Kruit, P. C. 1994, A&AS, 106, 451
- de Jong, R. S. 1996, A&A, 313, 377
- de Lapparent, V., Geller, M. J., & Huchra, J. P. 1989, ApJ, 343, 1
- de Vaucouleurs, G. 1977, in: *The Evolution of Galaxies and Stellar Populations*, eds. B. M. Tinsley & R. B. Larson, Yale University Observatory, New Haven, p. 43
- de Vaucouleurs, G., de Vaucouleurs, A., Corwin, H. G. Jr., Buta, R. J., Paturel, G., & Fouqué, P. 1991, *Third Reference Catalog of Bright Galaxies*, Springer-Verlag, New York (RC3)
- Ellis, R. S. 1997, ARA&A, 35, 389
- Ellis, R. S., Smail, I., Dressler, A., Couch, W. J., Oemler, A., Jr., Butcher, H., & Sharples, R. M. 1997, ApJ, 483, 582
- Fabricant, D., Cheimets, P., Caldwell, N., & Geary, J. 1998, PASP, 110, 79
- Franx, M., Illingworth, G., & Heckman, T. 1989, AJ, 98, 538
- Han, M. 1992, ApJS, 81, 35
- Hopp, U. 1999, A&AS, 134, 317
- Huchra, J. P., Davis, M., Latham, D., & Tonry, J. 1983, ApJS, 52, 89 (CfA I)
- 1997, (*CfA Redshift Catalog, version Feb 14 1997*)
- Jansen, R. A., Franx, M., Fabricant, D. G., & Caldwell, N. 1999, in preparation
- Johnson, H. L. 1955, Ann. Astrophys., 18, 292
- Jørgensen, I., Franx, M., & Kjærgaard, P. 1992, A&AS, 95, 489
- Kennicutt, R. C., Jr. 1992a, ApJ, 388, 310
- Kennicutt, R. C., Jr. 1992b, ApJS, 79, 255
- Kent, S. M. 1988, AJ, 96, 514
- Koo, D., & Kron, R. 1992, ARA&A, 30, 613
- Kraan-Korteweg, R. C., Sandage, A., & Tammann, G. A. 1984, ApJ, 283, 24
- van der Kruit, P. C. 1987, A&A, 173, 59
- Landolt, A. U. 1992, AJ, 104, 340
- Larson, R. B., & Tinsley, B. M. 1978, ApJ, 219, 46
- Marzke, R. O., Huchra, J. P., & Geller, M. J. 1994, ApJ, 428, 43
- McGaugh, S. S., Schombert, J. M., & Bothun, G. D. 1995, MNRAS, 280, 337
- Nilson, P. 1973, *Uppsala General Catalog of Galaxies*, Uppsala Astron. Obs. Ann. 6. (UGC)
- Patterson, R. J., & Thuan, T. X. 1996, ApJS, 107, 103
- Peletier, R. F., Davies, R. L., Illingworth, G. D., Davis, L. E., & Cawson, M. 1990, AJ, 100, 1091
- Persson, S. E., Frogel, J. Å., & Aaronson, M. 1979, ApJS, 39, 61
- Rieke, G. H., & Lebofsky, M. J. 1985, ApJ, 288, 618
- Sandage, A. 1972, ApJ, 176, 21
- Sandage, A., & Binggeli, B. 1984, AJ, 89, 919
- Sandage, A. R., & Visvanathan, N. 1978, ApJ, 223, 707
- Sprayberry, D., Impey, C. D., Bothun, G. D., & Irwin, M. J. 1995, AJ, 109, 558
- Swaters, R. A. 1998, private communication
- Swaters, R. A., & Balcells, M. 1999, in preparation (SB99)
- Tinsley, B. M. 1980, Fund. Cosmic Phys., 5, 287
- Tully, R. B., Verheijen, M. A. W., Pierce, M. J., Huang, J.-S., and Wainscoat, R. 1996, AJ, 112, 2471
- Yahil, A., Tammann, G. A., & Sandage, A. 1977, ApJ, 217, 903
- Zwicky, F., Herzog, E., Wild, P., Karpowicz, M., & Kowal, C. 1961–1968, *Catalog of Galaxies and of Clusters of Galaxies*, 6 vols., California Institute of Technology, Pasadena (CGCG)

APPENDIX

A. DISCUSSION OF INDIVIDUAL OBJECTS

- 006 A00510+1225** Compact Sc galaxy with Seyfert 1 nucleus. This galaxy was classified as compact elliptical in CfA I.
- 007 NGC 315** Aka. Holmberg 29A.
- 009 (A01047+1625)** This galaxy is not part of our statistical sample. It was observed because its estimated absolute magnitude was ~ -13 , making it a nice addition to our faintest bin in absolute magnitude. Recent observations by Hopp (1999), however, suggest a much larger distance, and therefore higher luminosity ($M_B \sim -14.5$), than adopted in this paper.
- 010 NGC 382** Close companion of NGC 383 in this group of galaxies.
- 011 IC 1639** Aka. Markarian 562.
- 012 A01123–0046** Compact Sc galaxy previously classified as compact elliptical in CfA I. This galaxy is interacting with two close companions.
- 018 A01374+1539B** This is the lowest surface brightness galaxy in our sample with a central surface brightness, $\mu_d^B(0) \sim 24.5$ mag arcsec $^{-2}$, and is also known as DDO 13.
- 027 NGC 927** Aka. Markarian 593.
- 031 A02464+1807** is a compact galaxy dominated by a foreground star right on its center. We succeeded neither in obtaining surface photometry of the underlying galaxy, nor spectroscopy for this galaxy. In the atlas we only show the image.
- 032 A02493–0122** is another LSB galaxy. Also known as DDO 30.
- 041 NGC 2799** VV 50, Arp 283; interacting pair with NGC 2798.
- 042 NGC 2824** Aka. Markarian 394. The light of a very bright star $\sim 3'$ away from the galaxy needed to be modelled out prior to the ellipse fitting step.

- 044 NGC 3011** Aka. Markarian 409.
- 047 A09557+4758** Through the irregular spiral disk of this galaxy, a more distant edge-on Sb is seen, giving the appearance of a break ($PA=42^\circ$) in one of the arms of A09557+4758.
- 050 NGC 3104** This LSB without a distinct nucleus is also known as VV 119.
- 052 NGC 3165** The central parts of this galaxy are distinctly asymmetric. Possible companion to the Northeast.
- 058 NGC 3279** Aka. IC 622.
- 059 A10321+4649** Aka. Markarian 146. Disturbed morphology with a dust lane.
- 062 A10365+4812** Galaxy showing the signature of a strongly warped disk.
- 063 A10368+4811** The light distribution in this galaxy is asymmetric.
- 064 NGC 3326** Aka. AKN 251. Very faint extended spiral structure is visible in this galaxy.
- 065 A10389+3859** Three smaller disk systems appear to accompany this galaxy.
- 066 A10431+3514** An edge-on early-type disk galaxy is seen through this Sa galaxy, $14''$ Northeast of the nucleus.
- 072 NGC 3499** A dustlane is running over this S0/a galaxy.
- 074 A11017+3828W** This is the nearest galaxy with a BL Lac type nucleus. It is highly variable (observed changes of ~ 0.02 mag per night during its high state in May 1996). The photometry presented in this paper is an average of observations from March 1995, and March and May 1996. Due to the brightness of this object (forcing us to use very short exposures) and due to the presence of two bright stars nearby (leading to inaccurate measurement of the sky background, even after modelling out the stellar light), our photometry of the host galaxy is not deep.
- 077 IC 673** Named IC 678 in CfA I. Galaxy with a low surface brightness disk and a normal surface brightness bulge.
- 079 A11072+1302** Contains multiple bright knots; peculiar galaxy, a likely merger.
- 080 NGC 3605** Light of the larger companion galaxy NGC 3607 needed to be modelled out prior to the ellipse fitting step.
- 088 A11336+5829** The positional angle listed in the UGC has an incorrect sign and should be -9° (or 171°) rather than 9° .
- 089 NGC 3795A** Named A1136+5833 in CfA I.
- 092 A11378+2840** Bright knots in the inner parts of an otherwise smooth galaxy.
- 093 A11392+1615** Aka. AKN 311 and Holmberg 275. May form a pair with a galaxy $2.3'$ to the West.
- 094 NGC 3846** Highly asymmetric light distribution. Outer parts look tidally disturbed.
- 097 NGC 3913** Aka. IC 740. The faint spiral structure appears to wind both clock- and counterclockwise.
- 105 A12001+6439** Aka. Markarian 195.
- 116 NGC 4288** Aka. DDO 119.
- 119 A12195+7535** Seyfert 1 galaxy Markarian 205, classified as compact elliptical, seen through the spiral disk of foreground galaxy NGC 4319.
- 120 A12263+4331** Aka. D 129.
- 130 NGC 4841B** Fainter of the two galaxies, to the northeast of brighter galaxy NGC 4841A. These two galaxies have a large overlap on the sky, resulting in shallow photometry.
- 151 NGC 5491** An apparent smaller companion is located $25''$ North of the nucleus.
- 152 NGC 5532** A smaller companion galaxy, $0.5'$ South of the center of this elliptical, is overlapping the outer parts.
- 153 NGC 5541** Aka. AKN 444.
- 154 NGC 5596** Aka. Markarian 470.
- 158 NGC 5762** This galaxy harbors a very extended and low surface brightness flocculent disk.
- 159 A14489+3547** This galaxy shows a highly warped, banana-shaped disk and forms a pair with A14492+3545. Also known as II Zw 70 and VV 324.
- 160 A14492+3545** Forms a pair with A14489+3547 (see remark above) and shows the morphological signature of a polar ring. Also known as II Zw 71 and VV 324.
- 161 IC 1066** A large barred spiral galaxy is located $2.1'$ North of this galaxy.
- 163 A15016+1037** Seyfert 1 nucleus. Also known as Markarian 841.
- 166 NGC 5875A** Named A1507+5229 in CfA I.
- 169 NGC 5940** Galaxy with a weak Seyfert 1 nucleus; also known as Markarian 9030.
- 171 NGC 5993** Two stars are superposed on this galaxy on either side of the nucleus. This galaxy as well as its neighbour $2.4'$ to the SW (not in this sample) show hints of tidal features and are probably in interaction.
- 173 IC 1144** Aka. Markarian 491.
- 175 A15523+1645** Aka. AKN 489.
- 181 NGC 7077** Aka. AKN 549.
- 183 A22306+0750** Also known as II Zw181 and AKN 558.
- 193 NGC 7620** Aka. Markarian 321.
- 194 A23264+1703** Harbors a double nucleus and shows tidal features of an ongoing interaction with a smaller companion.
- 196 NGC 7752** Strongly interacting companion of NGC 7753 with one of the tidally disrupted arms of NGC 7753 causing a starburst on one side of NGC 7752. Also known as AKN 585, IV Zw165 and VV 5.
- 197 A23514+2813** Named NGC 7777 in CfA I.
- (NGC 4319) Foreground spiral galaxy through which A12195+7535 is seen.

B. CALIBRATION OF THE INTENSITY PROFILES

We photometrically calibrated the radial intensity profiles by solving simultaneously for the calibration equations for B and R , or U and R , using $(B-R)$ and $(U-R)$ color terms, respectively. Consider the pair of calibration equations for the B and R intensity profiles:

$$\begin{cases} \mu_B(r) &= \mu_{B,i}(r) + pz_1 - pe_1 \cdot X_1 - pc_1 \cdot (\mu_B - \mu_R)(r) \\ \mu_R(r) &= \mu_{R,i}(r) + pz_2 - pe_2 \cdot X_2 - pc_2 \cdot (\mu_B - \mu_R)(r) \end{cases}, \quad (B1)$$

where $\mu_{\lambda,i}$ denotes the surface brightnesses in B and R in instrumental mag arcsec $^{-2}$, pz_n denote the photometric zero-points, pe_n the specific atmospheric extinction coefficients and X_n the airmass at the middle of the exposures, and pc_n denote the color term coefficients corresponding to our choice of reference filters.

If we denote by $P_n(r)$ the terms that are independent of color, $\mu_{\lambda,i}(r) + pz_n - pe_n \cdot X_n$, we can rewrite equations (B1) as

$$\begin{cases} (1 + pc_1) \cdot \mu_B(r) &= P_1(r) + pc_1 \cdot \mu_R(r) \\ (1 - pc_2) \cdot \mu_R(r) &= P_2(r) - pc_2 \cdot \mu_B(r) \end{cases}, \quad (B2)$$

from which we find after substitution of each of these equations into each other:

$$\mu_B(r) = \frac{(1 - pc_2) \cdot P_1 + pc_1 \cdot P_2}{1 + pc_1 - pc_2} \quad \text{and} \quad \mu_R(r) = \frac{(1 + pc_1) \cdot P_2 - pc_2 \cdot P_1}{1 + pc_1 - pc_2}. \quad (B3)$$

Equations (B3) represent the solutions for the surface brightness profiles, corrected for the color term, in each of the two filters. Similar equations hold for U and R and corresponding color $(U-R)$. This procedure avoids the introduction of additional correlated errors in the radial surface brightness profiles due to the two filters used in the color term correction, that one expects when propagating errors in the more commonly applied iterative methods.

For completeness we give also the equations used to find the formal random errors on the surface brightness profiles thus derived:

$$\begin{cases} nm &= 1 + pc_1 - pc_2 \\ \sigma_{\mu_B}(r) &= \frac{1}{nm} \cdot \sqrt{(1 - pc_2)^2 \sigma_{P_1}^2 + pc_1^2 \sigma_{P_2}^2 + (\mu_B^2(r) + P_1^2) \cdot \sigma_{pc_2}^2 + (\mu_B^2(r) + P_2^2) \cdot \sigma_{pc_1}^2} \\ \sigma_{\mu_R}(r) &= \frac{1}{nm} \cdot \sqrt{(1 + pc_1)^2 \sigma_{P_2}^2 + pc_2^2 \sigma_{P_1}^2 + (\mu_R^2(r) + P_1^2) \cdot \sigma_{pc_2}^2 + (\mu_R^2(r) + P_2^2) \cdot \sigma_{pc_1}^2} \end{cases}. \quad (B4)$$

The third and fourth terms under the root-sign are the dominant ones. We assume here that the individual errors, σ , are Gaussian in nature, and un-correlated. This approximately holds at the level of accuracy we are aiming for in this work.

For the non-photometric profiles that were scaled to photometric intensity levels, we use the calibration constants, airmass and pixel scale of the photometric reference profile. The error on the fitted scale factor is included in quadrature in the error propagation.

All unique B,R -filter pairs of intensity profiles were calibrated as described above, after which multiple resulting surface brightness profiles were combined into a single profile per filter. In the U calibration we paired all U filter intensity profiles with a corresponding R profile, but only solved for the U filter part of equations (B3), not the R filter one, as the B filter profiles had better S/N in general and were therefore better suited for this purpose.

TABLE 3
PHOTOMETRIC MEASUREMENTS AND PARAMETERS.

ID	Name	UGC # (1)	Dist Mpc (2)	B_{tot} (mag) (5)	M_B^{tot} (mag) (6)	r_{26}^B ($\prime\prime$) (7)	B_{26} (mag) (8)	r_e^B ($\prime\prime$) (9)	μ_e^B (mag/ \square^2) (10)	$(U-B)_e$ (mag) (11)	$(B-R)_e$ (mag) (12)	$\Delta(U-B)^\dagger$ (mag) (13)	$\Delta(B-R)^\dagger$ (mag) (14)
1	A00113p3037	130	48.6	14.66±0.02	-18.77±0.09	32.19± 4.29	14.76±0.03	6.26±0.04	21.68±0.03	0.53±0.02	1.52±0.02	-0.05±0.03	-0.17±0.03
2	A00289p0556	313	20.9	14.48±0.01	-17.12±0.20	31.44± 1.91	14.52±0.01	9.17±0.04	21.79±0.02	-0.16±0.01	0.88±0.01	0.16±0.03	0.05±0.02
3	NGC193	408	43.2	12.93±0.03	-20.25±0.10	89.42±14.28	13.08±0.05	27.92±0.38	23.41±0.08	0.56±0.04	1.53±0.03	-0.11±0.07	-0.16±0.06
4	A00389m0159	439	52.4	13.79±0.01	-19.81±0.08	46.21± 2.94	13.86±0.01	11.71±0.05	22.08±0.02	0.00±0.01	1.06±0.01	-0.15±0.03	-0.16±0.02
5	A00442p3224	484	49.7	13.89±0.02	-19.59±0.09	50.98± 3.99	13.96±0.02	17.16±0.20	22.80±0.06	0.25±0.03	1.35±0.03	-0.30±0.05	-0.39±0.05
6	A00510p1225	545	182.8	14.30±0.01	-22.01±0.03	20.88± 1.84	14.32±0.01	1.19±0.01	17.40±0.01	-0.22±0.12	0.73±0.02	-0.51±0.26	-0.11±0.04
7	NGC315	597	50.5	12.04±0.04	-21.48±0.09	112.14±17.37	12.13±0.04	29.52±0.43	22.50±0.09	0.57±0.04	1.55±0.04	-0.16±0.08	-0.08±0.07
8	A00570p1504	615	55.3	14.70±0.02	-19.01±0.08	26.60± 1.80	14.75±0.01	7.48±0.09	22.18±0.04	0.43±0.02	1.53±0.02	-0.31±0.03	-0.30±0.03
9	(A01047p1625	685	3.0	14.09±0.02	-13.33±1.10	53.31± 4.42	14.23±0.03	20.31±0.14	23.24±0.04	-0.16±0.03	0.79±0.03	0.28±0.06	0.16±0.04
10	NGC382	688	53.2	14.56±0.06	-19.07±0.10	27.99± 1.98	14.63±0.03	6.58±0.09	21.73±0.06	0.64±0.06	1.57±0.06	0.04±0.11	-0.10±0.10
11	IC1639	750	53.2	14.38±0.01	-19.25±0.08	26.28± 2.47	14.42±0.01	4.23±0.05	20.54±0.02	0.36±0.01	1.31±0.01	0.02±0.02	-0.12±0.02
12	A01123m0046	793	102.8	14.81±0.01	-20.25±0.04	23.33± 1.62	14.84±0.01	7.59±0.02	21.66±0.02	-0.05±0.01	1.18±0.01	-0.05±0.02	-0.21±0.02
13	A01187m0048	892	51.6	13.68±0.02	-19.88±0.08	63.10± 5.32	13.78±0.02	23.16±0.22	23.31±0.06	0.37±0.03	1.38±0.02	-0.23±0.05	-0.29±0.04
14	NGC516	946	24.4	14.34±0.02	-17.60±0.17	39.02± 4.63	14.42±0.02	9.99±0.07	22.15±0.02	0.39±0.02	1.46±0.02	-0.03±0.04	-0.05±0.04
15	A01300p1804	1104	8.0	14.33±0.01	-15.19±0.48	37.25± 3.01	14.41±0.01	10.73±0.04	22.21±0.02	-0.27±0.02	0.70±0.01	0.16±0.03	0.19±0.03
16	A01344p2838	1154	78.0	14.64±0.02	-19.82±0.06	26.44± 1.52	14.67±0.01	7.72±0.06	21.80±0.03	-0.05±0.02	1.03±0.02	-0.24±0.04	-0.22±0.04
17	A01346p0438	1155	31.3	14.79±0.01	-17.69±0.13	23.36± 1.83	14.83±0.01	5.33±0.02	21.10±0.02	-0.15±0.01	0.94±0.01	-0.03±0.02	-0.11±0.02
18	A01374p1539	1176	7.3	14.09±0.09	-15.23±0.53	74.31±12.74	14.53±0.14	55.23±3.14	25.37±0.32	0.52±0.11	0.29±0.19
19	NGC695	1315	98.5	13.97±0.03	-21.00±0.05	30.34± 4.06	14.07±0.01	7.19±0.05	20.91±0.02	-0.07±0.03	1.22±0.03	-0.03±0.05	-0.15±0.05
20	(NGC784)	1501	3.6	12.23±0.05	-15.56±0.96	113.27±13.46	12.33±0.05	42.93±0.76	23.03±0.10	-0.26±0.05	0.71±0.05	0.15±0.08	0.06±0.09
21	A02008p2350	1551	27.3	13.55±0.04	-18.63±0.16	72.67± 8.03	13.63±0.03	31.94±0.35	23.53±0.06	-0.07±0.05	0.91±0.05	-0.10±0.09	-0.20±0.09
22	IC195	1555	36.5	14.20±0.04	-18.61±0.12	36.86± 6.91	14.34±0.03	7.79±0.04	21.83±0.02	0.19±0.04	1.52±0.04	-0.26±0.07	-0.09±0.07
23	IC197	1564	62.4	14.49±0.01	-19.49±0.07	25.07± 1.54	14.51±0.01	9.12±0.04	21.79±0.03	0.07±0.01	1.18±0.01	-0.28±0.02	-0.33±0.02
24	IC1776	1579	33.6	14.08±0.02	-18.55±0.13	51.38± 3.29	14.15±0.02	21.70±0.19	23.39±0.05	-0.08±0.03	0.88±0.02	-0.07±0.05	-0.15±0.04
25	A02056p1444	1630	43.9	13.94±0.04	-19.27±0.10	42.79±11.69	14.17±0.05	11.72±0.10	21.90±0.04	-0.01±0.04	1.11±0.04	-0.00±0.06	-0.14±0.06
26	NGC825	1636	33.6	14.10±0.02	-18.53±0.13	44.90± 3.99	14.21±0.02	10.31±0.11	22.50±0.03	0.50±0.02	1.61±0.02	-0.25±0.05	-0.20±0.04
27	NGC927	1908	81.9	13.84±0.01	-20.73±0.05	44.29± 2.64	13.87±0.01	16.28±0.08	22.45±0.03	0.07±0.02	1.24±0.01	-0.11±0.03	-0.27±0.03
28	A02257m0134	1945	17.1	14.12±0.02	-17.05±0.24	49.32± 4.70	14.23±0.02	17.98±0.13	22.95±0.04	-0.11±0.02	0.98±0.02	0.11±0.04	0.11±0.04
29	NGC984	2059	44.2	13.62±0.04	-19.61±0.10	58.36± 9.81	13.72±0.05	18.47±0.34	22.91±0.11	0.58±0.05	1.68±0.04	-0.23±0.08	-0.26±0.08
30	NGC1029	2149	36.0	13.93±0.02	-18.85±0.12	34.21± 5.84	13.99±0.02	7.65±0.04	21.15±0.03	0.59±0.02	1.63±0.02	0.04±0.04	-0.16±0.04
31	A02464p1807	2296	101.0	13.26±0.04	-21.76±0.06	48.69± 8.68	13.31±0.04	2.37±0.28	18.42±0.09	0.91±0.05	1.18±0.11	0.09±0.11	0.06±0.27
32	A02493m0122	2345	14.6	14.27±0.05	-16.55±0.28	70.00± 5.23	14.46±0.05	40.68±0.85	24.71±0.14	0.12±0.07	0.84±0.07	-0.10±0.12	-0.12±0.13
33	NGC1298	2683	63.9	14.01±0.03	-20.02±0.07	45.83± 7.29	14.09±0.04	10.96±0.10	22.28±0.05	0.64±0.04	1.53±0.03	-0.02±0.08	-0.05±0.06
34	A03202m20205	2704	80.7	14.33±0.02	-20.21±0.06	38.08± 3.89	14.42±0.02	8.88±0.06	21.81±0.02	0.16±0.02	1.48±0.02	-0.17±0.03	-0.22±0.04
35	NGC1552	3015	48.0	13.47±0.06	-19.93±0.11	69.82±13.94	13.63±0.06	19.54±0.34	23.16±0.08	0.54±0.06	1.68±0.06	-0.04±0.10	-0.19±0.10
36	NGC2692	4675	40.3	14.04±0.03	-18.99±0.11	39.46± 7.56	14.16±0.03	10.56±0.08	22.03±0.04	0.50±0.03	1.71±0.03	-0.09±0.06	-0.09±0.05
37	A08567p5242	4713	92.3	13.90±0.03	-20.93±0.06	50.21± 3.16	14.01±0.01	17.75±0.18	22.95±0.03	0.26±0.04	1.54±0.04	-0.18±0.06	-0.28±0.06
38	A09045p3328	4787	6.1	14.44±0.02	-14.48±0.62	39.32± 2.42	14.49±0.02	15.71±0.13	22.87±0.05	-0.09±0.03	0.86±0.02	-0.00±0.04	0.01±0.04
39	NGC2780	4843	22.0	14.52±0.02	-17.19±0.19	31.77± 1.65	14.57±0.01	12.70±0.06	22.31±0.03	0.07±0.02	1.32±0.02	-0.11±0.04	-0.15±0.04
40	A09125p5303	4879	8.2	13.67±0.04	-15.90±0.48	72.10± 8.16	13.83±0.04	31.69±0.54	23.92±0.09	0.01±0.05	1.16±0.04	0.20±0.08	0.28±0.07
41	NGC2799	4909	21.6	14.26±0.06	-17.42±0.20	36.33± 1.96	14.45±0.01	12.32±0.11	22.67±0.04	-0.09±0.06	1.07±0.06	0.09±0.11	-0.09±0.11
42	NGC2824	4933	29.5	13.38±0.08	-18.97±0.16	78.16±23.99	13.78±0.15	35.34±1.52	24.89±0.24	0.49±0.08	1.52±0.09	0.85±0.14	-0.04±0.16
43	NGC2844	4971	17.7	13.77±0.02	-17.47±0.23	49.34± 3.94	13.86±0.02	12.63±0.07	22.28±0.02	0.20±0.02	1.45±0.02	-0.07±0.03	-0.21±0.04
44	NGC3011	5259	18.0	14.65±0.01	-16.62±0.23	27.89± 1.88	14.69±0.01	6.32±0.09	21.46±0.04	-0.16±0.02	1.25±0.01	-0.03±0.03	-0.20±0.03
45	NGC3009	5264	49.0	14.67±0.02	-18.78±0.09	30.40± 2.00	14.70±0.01	11.63±0.05	22.32±0.03	0.06±0.02	1.11±0.02	-0.10±0.04	-0.16±0.03
46	IC2520	5335	14.8	14.03±0.03	-16.82±0.28	32.74± 3.91	14.17±0.01	10.07±0.04	21.74±0.02	-0.20±0.03	1.26±0.03	-0.24±0.07	-0.27±0.05
47	A09557p4758	5354	15.0	13.69±0.05	-17.19±0.28	65.51±12.72	13.89±0.07	27.97±0.40	23.61±0.08	-0.23±0.05	0.81±0.05	-0.00±0.09	-0.22±0.09
48	NGC3075	5360	37.1	14.07±0.02	-18.78±0.12	46.42± 5.58	14.17±0.03	17.47±0.11	22.88±0.04	-0.02±0.02	1.15±0.02	-0.17±0.04	-0.28±0.04
49	A09579p0439	5378	42.7	14.73±0.02	-18.42±0.10	31.27± 1.63	14.78±0.01	9.22±0.06	22.28±0.03	0.09±0.02	1.18±0.02	-0.08±0.05	-0.25±0.03
50	NGC3104	5414	7.1	13.30±0.04	-15.96±0.54	81.74± 7.58	13.41±0.04	23.95±0.10	22.74±0.10	-0.27±0.04	0.79±0.04	0.01±0.07	0.07±0.07
51	A10042p4716	5451	7.2	14.13±0.02	-15.17±0.53	49.49± 3.51	14.25±0.02	17.76±0.15	22.89±0.05	-0.08±0.02	1.18±0.02	-0.00±0.04	-0.03±0.04
52	NGC3165	5512	14.8	14.57±0.02	-16.28±0.28	37.13± 2.61	14.64±0.02	14.71±0.14	22.80±0.06	-0.02±0.03	1.11±0.02	-0.06±0.05	-0.02±0.04
53	A10114p0716	5522	14.0	13.82±0.05	-16.90±0.30	72.14± 5.52	13.99±0.03	28.48±0.61	24.40±0.10	-0.24±0.05	0.89±0.05	-0.24±0.10	-0.32±0.09
54	NGC3179	5555	74.7	14.29±0.01	-20.08±0.06	32.47± 2.24	14.36±0.01	6.81±0.11	21.57±0.05	0.67±0.03	1.56±0.02	-0.05±0.06	-0.09±0.03
55	A10171p3853	5577	23.3	14.45±0.02	-17.38±0.18	34.39± 2.32	14.50±0.02	13.57±0.16	22.64±0.05	-0.17±0.02	0.96±0.02	-0.05±0.04	-0.05±0.03
56	NGC3213	5590	16.8	13.95±0.07	-17.18±0.25	40.20± 4							

TABLE 3—Continued

ID	Name	UGC #	Dist Mpc	B_{tot} (mag)	M_B^{tot} (mag)	r_{26}^B ('')	B_{26} (mag)	r_e^B ('')	μ_e^B (mag/ \square^2)	$(U-B)_e$ (mag)	$(B-R)_e$ (mag)	$\Delta(U-B)^\dagger$ (mag)	$\Delta(B-R)^\dagger$ (mag)
(1)	(2)	(3)	(4)	(5)	(6)	(7)	(8)	(9)	(10)	(11)	(12)	(13)	(14)
81	A11142p1804	6296	9.1	14.46±0.02	-15.32±0.43	36.07± 2.54	14.53±0.01	13.49±0.07	22.55±0.03	0.19±0.02	1.40±0.02	-0.07±0.04	-0.12±0.03
82	NGC3633	6351	27.7	14.01±0.18	-18.20±0.24	30.31± 5.30	14.46±0.02	13.31±0.12	22.66±0.05	0.28±0.18	1.51±0.18	-0.02±0.31	-0.44±0.31
83	IC692	6438	15.0	14.60±0.01	-16.28±0.27	26.03± 2.28	14.64±0.01	5.22±0.02	21.11±0.02	-0.19±0.01	0.76±0.01	0.10±0.03	0.18±0.02
84	A11238p5401	6446	9.0	13.35±0.11	-16.43±0.45	91.32±14.01	13.64±0.08	51.47±1.60	24.74±0.18	-0.18±0.11	0.80±0.11	-0.07±0.20	-0.21±0.20
85	A11310p3254	6545	29.5	14.37±0.02	-17.98±0.14	33.60± 3.82	14.42±0.02	10.87±0.04	21.89±0.02	0.21±0.02	1.36±0.02	-0.13±0.04	-0.23±0.04
86	IC708	6549	95.0	14.21±0.02	-20.68±0.05	50.50± 5.66	14.39±0.04	15.94±0.13	23.55±0.04	0.52±0.03	1.64±0.02	-0.05±0.05	-0.08±0.04
87	A11332p3536	6570	20.0	14.33±0.01	-17.17±0.21	34.14± 3.17	14.40±0.01	6.73±0.04	21.57±0.03	0.08±0.02	1.20±0.01	0.14±0.03	0.03±0.03
88	A11336p5829	6575	16.3	14.33±0.03	-16.73±0.25	37.16± 3.94	14.39±0.02	13.64±0.10	22.51±0.04	-0.19±0.03	0.92±0.03	-0.09±0.05	-0.17±0.05
89	NGC3795A	6616	15.6	13.65±0.03	-17.31±0.26	74.49± 4.03	13.74±0.02	33.86±0.41	23.94±0.07	-0.00±0.03	0.92±0.03	-0.10±0.06	-0.17±0.05
90	A11372p2012	6625	108.9	14.30±0.02	-20.89±0.04	27.39± 1.04	14.34±0.01	8.64±0.03	21.51±0.02	-0.05±0.02	1.02±0.02	-0.23±0.03	-0.35±0.03
91	NGC3795	6629	14.9	14.10±0.02	-16.77±0.27	39.93± 3.64	14.15±0.02	13.09±0.08	22.27±0.04	0.08±0.02	1.19±0.02	-0.15±0.04	-0.19±0.04
92	A11378p2840	6637	22.0	14.84±0.01	-16.88±0.19	23.16± 1.40	14.90±0.01	5.07±0.02	20.95±0.01	-0.16±0.01	0.91±0.01	-0.03±0.03	0.03±0.02
93	A11392p1615	6655	6.2	14.85±0.02	-14.11±0.61	27.04± 2.81	14.90±0.01	5.89±0.04	21.51±0.03	-0.26±0.02	0.83±0.02	0.25±0.05	-0.00±0.03
94	NGC3846	6706	18.1	13.78±0.03	-17.51±0.23	61.12± 3.52	13.86±0.02	21.40±0.24	23.30±0.06	-0.09±0.03	0.83±0.03	-0.10±0.06	-0.07±0.05
95	NGC3850	6733	15.7	13.94±0.02	-17.04±0.26	59.07± 3.30	14.04±0.02	24.48±0.21	23.45±0.05	-0.06±0.03	0.94±0.02	-0.09±0.05	-0.11±0.04
96	A11476p4220	6805	14.2	14.85±0.01	-15.91±0.29	22.60± 2.48	14.90±0.01	4.75±0.03	21.01±0.01	-0.16±0.01	0.99±0.01	0.35±0.02	0.11±0.02
97	NGC3913	6813	13.4	13.23±0.08	-17.40±0.31	87.59±14.18	13.44±0.07	39.33±0.92	24.29±0.15	-0.10±0.08	1.00±0.08	-0.11±0.14	-0.20±0.14
98	IC746	6898	52.7	14.73±0.02	-18.88±0.08	28.87± 3.26	14.79±0.02	8.02±0.03	21.89±0.02	-0.04±0.02	0.92±0.02	-0.14±0.04	-0.10±0.03
100	NGC3978	6903	21.9	13.53±0.06	-18.17±0.20	72.80± 5.03	13.60±0.02	37.09±0.30	23.68±0.05	-0.03±0.06	1.06±0.06	-0.16±0.10	-0.25±0.10
101	A11547p4933	6930	10.8	12.71±0.08	-17.45±0.38	106.62±16.90	12.88±0.08	47.41±1.81	23.63±0.23	-0.08±0.09	0.96±0.09	-0.15±0.16	-0.19±0.15
102	A11547p5813	6931	15.9	14.66±0.02	-16.34±0.26	39.02± 2.12	14.73±0.02	17.13±0.11	23.14±0.04	-0.25±0.03	0.72±0.03	-0.21±0.05	-0.12±0.04
103	NGC4034	7006	27.8	14.44±0.04	-17.78±0.16	48.68± 2.42	14.50±0.02	21.41±0.22	23.63±0.06	0.05±0.04	1.13±0.04	-0.10±0.07	-0.23±0.06
104	A11592p6237	7009	15.3	14.56±0.02	-16.37±0.27	33.63± 1.61	14.61±0.02	13.65±0.11	22.88±0.05	-0.28±0.02	0.77±0.02	0.05±0.04	-0.04±0.04
105	A12001p6439	7020A	18.7	14.45±0.02	-16.91±0.22	29.76± 3.22	14.49±0.01	5.96±0.04	21.40±0.03	-0.16±0.02	1.20±0.02	-0.01±0.03	-0.19±0.03
106	NGC4117	7112	13.3	14.01±0.01	-16.61±0.30	41.87± 4.07	14.07±0.02	10.08±0.04	21.92±0.02	0.30±0.02	1.51±0.01	-0.09±0.03	-0.17±0.03
107	NGC4120	7121	26.5	14.22±0.03	-17.90±0.16	39.96± 4.48	14.29±0.02	14.35±0.10	22.51±0.04	-0.19±0.03	0.98±0.03	-0.03±0.05	-0.08±0.05
108	A12064p4201	7129	12.8	14.21±0.02	-16.33±0.31	44.48± 3.13	14.30±0.02	13.25±0.08	0.03±0.02	1.25±0.02	0.29±0.03	0.12±0.03	
109	NGC4141	7147	23.9	13.53±0.05	-18.36±0.18	46.84± 3.83	13.60±0.04	14.62±0.28	22.05±0.12	0.64±0.05	1.16±0.05	-0.24±0.08	-0.36±0.09
110	NGC4159	7174	21.7	14.26±0.01	-17.42±0.19	36.88± 3.61	14.33±0.02	11.62±0.07	22.19±0.03	-0.16±0.02	0.99±0.02	-0.02±0.03	-0.06±0.03
111	NGC4204	7261	7.1	12.87±0.07	-16.38±0.55	112.40±20.32	13.15±0.10	61.49±3.01	24.63±0.30	-0.18±0.09	0.86±0.08	0.01±0.15	-0.18±0.14
112	NGC4238	7308	31.6	14.25±0.01	-18.25±0.13	35.04± 1.41	14.29±0.01	13.46±0.05	22.33±0.02	-0.19±0.02	0.87±0.02	-0.05±0.03	-0.09±0.03
113	NGC4248	7335	6.0	13.30±0.02	-15.59±0.62	70.36± 6.07	13.38±0.02	25.93±0.30	23.06±0.06	0.10±0.03	1.36±0.02	0.15±0.05	0.10±0.04
114	A12167p4938	7358	39.9	14.34±0.01	-18.67±0.11	33.16± 1.60	14.37±0.02	14.29±0.09	22.45±0.04	0.19±0.02	1.18±0.02	-0.20±0.04	-0.27±0.03
115	NGC4272	7378	86.9	14.20±0.03	-20.50±0.06	50.57± 5.77	14.35±0.04	14.79±0.28	23.24±0.10	0.52±0.04	1.63±0.03	-0.11±0.07	-0.08±0.06
116	NGC4288	7399	6.5	13.39±0.02	-15.68±0.58	65.57± 5.75	13.47±0.02	25.01±0.22	22.94±0.05	-0.23±0.03	0.80±0.03	-0.11±0.05	-0.11±0.05
117	NGC4308	7426	5.9	14.41±0.01	-14.44±0.63	31.11± 2.24	14.48±0.01	7.83±0.04	21.81±0.02	0.32±0.02	1.39±0.01	-0.11±0.03	-0.14±0.03
118	A12195p3222	7428	16.5	14.01±0.04	-17.07±0.25	53.46± 7.64	14.22±0.04	24.04±0.40	23.68±0.10	-0.01±0.04	0.79±0.04	0.02±0.08	-0.10±0.08
119	A12195p7535	7449	21.4	14.49±0.04	-21.16±0.04	11.07± 0.66	15.51±0.03	1.77±0.06	19.39±0.08	-1.01±0.05	0.73±0.07	0.02±0.10	0.09±0.16
120	A12263p4331	7608	6.2	13.85±0.08	-15.12±0.61	77.70±14.63	14.28±0.13	55.27±2.61	25.23±0.30	-0.22±0.09	0.70±0.10	-0.02±0.17	-0.15±0.17
121	A12295p4007	7678	7.8	14.15±0.02	-15.32±0.49	41.48± 2.61	14.24±0.01	12.55±0.10	22.30±0.04	-0.33±0.02	0.62±0.02	0.11±0.03	0.18±0.03
122	A12300p4259	7690	6.2	13.37±0.01	-15.61±0.60	63.72± 2.17	13.41±0.01	21.50±0.12	22.71±0.03	-0.22±0.02	0.82±0.01	-0.15±0.03	-0.10±0.03
123	A12304p43754	7699	5.3	13.25±0.01	-15.35±0.70	67.48± 2.67	13.30±0.01	27.08±0.14	22.90±0.03	-0.19±0.02	0.81±0.01	-0.10±0.03	-0.16±0.02
124	NGC4509	7704	12.0	14.39±0.02	-16.01±0.33	30.29± 2.48	14.44±0.01	8.13±0.05	21.50±0.04	-0.47±0.02	0.52±0.02	0.07±0.04	0.05±0.03
125	A12331p7230	7761	72.8	14.64±0.02	-19.67±0.06	26.86± 2.34	14.67±0.01	9.86±0.05	22.19±0.04	-0.01±0.02	1.10±0.02	-0.05±0.04	-0.14±0.04
126	A12446p5155	7950	6.9	13.44±0.07	-15.77±0.55	72.73±13.51	13.60±0.07	25.60±0.81	23.68±0.20	-0.21±0.08	0.66±0.08	0.28±0.13	0.01±0.14
127	NGC4758	8014	17.3	13.56±0.04	-17.64±0.24	61.41± 5.39	13.62±0.03	24.56±0.25	23.09±0.06	0.11±0.04	1.12±0.04	-0.03±0.07	-0.11±0.07
128	NGC4795	8037	31.0	13.00±0.01	-19.46±0.14	70.66± 3.90	13.06±0.01	21.21±0.15	22.73±0.03	0.44±0.02	1.49±0.01	-0.10±0.03	-0.13±0.03
129	NGC4807	8049	72.0	14.58±0.02	-19.71±0.06	34.43± 2.57	14.66±0.01	7.12±0.05	22.04±0.02	0.49±0.02	1.57±0.02	-0.11±0.03	-0.14±0.03
130	NGC4841B	8073	65.4	14.69±0.03	-19.39±0.07	29.81± 1.66	14.76±0.02	8.03±0.09	22.22±0.06	0.56±0.03	1.54±0.03	-0.12±0.06	-0.15±0.06
131	NGC4926	8142	80.1	14.05±0.02	-20.47±0.06	46.53± 4.86	14.20±0.03	12.46±0.09	22.77±0.03	0.57±0.02	1.60±0.02	-0.14±0.04	-0.10±0.04
132	NGC4961	8185	29.1	13.75±0.02	-18.57±0.15	45.66± 3.70	13.81±0.01	14.19±0.14	22.50±0.05	-0.08±0.03	0.93±0.02	-0.19±0.05	-0.21±0.04
133	A13065p5420	8231	28.7	14.55±0.02	-17.74±0.15	32.95± 2.10	14.59±0.02	13.03±0.08	22.62±0.04	-0.22±0.02	0.77±0.02	0.16±0.03	0.19±0.03
134	IC4213	8280	10.4	14.06±0.01	-16.03±0.38	42.34± 2.14	14.12±0.01	15.37±0.10	22.52±0.03	-0.12±0.02	0.94±0.01	0.01±0.03	-0.09±0.02
135	A13194p4232	8400	37.7	14.57±0.02	-18.31±0.11	28.56± 1.39	14.60±0.01	10.41±0.04	22.05±0.02	-0.08±0.02	1.10±0.03	-0.10±0.04	-0.17±0.06
136	NGC5117	8411	28.0	14.29±0.04	-17.95±0.15	45.91± 2.45	14.34±0.03	18.50±0.35	23.37±0.10	0.29±0.04	0.99±0.04	-0.12±0.07	-0.15±0.07
137	NGC5												

TABLE 3—Continued

ID	Name	UGC	Dist	B_{tot}	M_B^{tot}	r_{26}^B	B_{26}	r_e^B	μ_e^B	$(U-B)_e$	$(B-R)_e$	$\Delta(U-B)^\dagger$	$\Delta(B-R)^\dagger$
(1)	(2)	#	Mpc	(mag)	(mag)	($''$)	(mag)	($''$)	(mag/ \square^2)	(mag)	(mag)	(mag)	(mag)
		(3)	(4)	(5)	(6)	(7)	(8)	(9)	(10)	(11)	(12)	(13)	(14)
161	IC1066	9573	19.6	13.87±0.02	-17.59±0.21	42.32± 3.54	13.92±0.02	13.23±0.09	22.10±0.03	0.08±0.03	1.16±0.02	-0.18±0.05	-0.28±0.03
162	A14594p4454	9660	9.8	14.33±0.01	-15.62±0.40	31.15± 3.13	14.38±0.01	7.69±0.02	21.34±0.02	-0.29±0.02	0.65±0.01	-0.02±0.03	0.07±0.02
163	A15016p1037	...	109.5	14.80±0.03	-20.40±0.05	17.27± 2.13	14.83±0.03	1.43±0.05	18.30±0.12	-0.48±0.11	0.76±0.06	-0.65±0.20	-0.06±0.12
164	IC1100	9729	69.2	14.20±0.02	-20.00±0.07	33.33± 1.93	14.27±0.01	10.62±0.05	21.86±0.03	0.12±0.02	1.23±0.02	-0.11±0.03	-0.19±0.03
165	NGC5874	9736	35.4	13.63±0.06	-19.12±0.13	60.92± 5.46	13.70±0.03	28.61±0.24	23.18±0.06	0.07±0.07	1.35±0.06	-0.19±0.11	-0.16±0.11
166	NGC5875A	9741	29.0	14.51±0.01	-17.80±0.15	34.96± 2.24	14.58±0.01	9.95±0.04	21.84±0.03	-0.24±0.02	0.86±0.01	-0.06±0.03	-0.01±0.03
167	NGC5888	9771	90.7	14.15±0.06	-20.64±0.08	39.55± 3.52	14.23±0.04	14.32±0.23	22.48±0.11	0.45±0.06	1.53±0.06	-0.30±0.10	-0.25±0.10
168	IC1124	9869	55.7	14.58±0.01	-19.15±0.08	24.64± 1.47	14.60±0.01	7.89±0.03	21.54±0.03	0.18±0.02	1.39±0.01	-0.11±0.03	-0.25±0.02
169	NGC5940	9876	101.9	14.49±0.02	-20.55±0.05	30.00± 1.35	14.53±0.02	10.65±0.09	22.16±0.04	-0.05±0.04	1.20±0.02	-0.09±0.08	-0.19±0.04
170	A15314p6744	9896	68.2	14.39±0.02	-19.78±0.07	37.96± 1.73	14.42±0.02	15.11±0.10	22.73±0.04	...	1.25±0.02	...	-0.30±0.04
171	NGC5993	10007	97.5	14.01±0.03	-20.93±0.05	43.53± 6.78	14.09±0.03	11.41±0.18	22.01±0.02	-0.09±0.04	1.03±0.03	0.04±0.07	-0.08±0.06
172	IC1141	10051	47.6	14.77±0.02	-18.62±0.09	23.53± 0.99	14.80±0.01	5.68±0.11	21.84±0.03	0.08±0.02	1.35±0.02	0.02±0.03	-0.03±0.04
173	IC1144	10069	122.8	14.81±0.02	-20.64±0.04	29.39± 3.81	14.89±0.02	5.79±0.15	21.76±0.03	0.19±0.05	1.46±0.02	-0.21±0.06	-0.17±0.04
174	NGC6007	10079	106.3	14.02±0.03	-21.11±0.05	42.41± 3.03	14.06±0.02	16.93±0.13	22.60±0.05	0.15±0.04	1.27±0.03	-0.28±0.06	-0.39±0.05
175	A15523p1645	10086	25.7	14.92±0.07	-17.13±0.18	20.69± 2.21	15.12±0.01	5.84±0.03	21.38±0.03	0.04±0.09	1.01±0.07	-0.01±0.16	-0.09±0.12
176	A15542p4800	10097	63.6	13.68±0.03	-20.34±0.07	60.66± 9.29	13.84±0.04	15.36±0.13	22.94±0.04	0.56±0.03	1.59±0.03	-0.10±0.05	-0.20±0.06
177	NGC6020	10100	47.3	13.73±0.03	-19.65±0.09	56.11± 7.94	13.89±0.04	14.45±0.09	22.77±0.03	0.56±0.03	1.58±0.03	-0.09±0.05	-0.08±0.05
178	NGC6123	10333	43.8	14.71±0.02	-18.50±0.10	24.29± 3.86	14.77±0.02	5.38±0.02	21.08±0.02	0.58±0.02	1.55±0.02	-0.11±0.03	-0.10±0.03
179	NGC6131	10356	54.2	13.92±0.11	-19.75±0.14	51.44± 6.83	14.04±0.07	20.11±0.62	22.88±0.20	-0.11±0.11	1.08±0.11	-0.03±0.18	-0.16±0.18
180	NGC6185	10444	104.9	13.77±0.03	-21.33±0.05	56.25± 4.62	13.92±0.02	15.49±0.10	22.77±0.03	0.45±0.03	1.50±0.03	-0.16±0.05	-0.18±0.04
181	NGC7077	11755	13.2	14.44±0.02	-16.17±0.31	33.32± 3.88	14.50±0.02	7.04±0.05	21.72±0.03	-0.30±0.02	0.78±0.02	0.22±0.05	0.28±0.04
182	NGC7194	11888	82.4	13.72±0.03	-20.86±0.06	60.56± 8.04	13.88±0.04	15.65±0.13	23.07±0.04	0.57±0.03	1.60±0.03	-0.09±0.06	-0.08±0.05
183	A22306p0750	12074	21.3	14.30±0.04	-17.34±0.20	25.34± 2.34	14.38±0.01	8.11±0.03	21.22±0.02	0.00±0.04	1.15±0.04	-0.06±0.06	-0.11±0.06
184	NGC7328	12118	29.5	13.82±0.02	-18.53±0.14	42.29± 2.45	13.86±0.01	14.33±0.08	22.15±0.03	0.23±0.02	1.41±0.02	-0.07±0.03	-0.13±0.03
185	NGC7360	12167	47.6	14.59±0.02	-18.80±0.09	32.38± 4.19	14.66±0.02	8.23±0.04	21.96±0.02	0.36±0.02	1.45±0.02	-0.17±0.04	-0.18±0.03
186	A22426p0610	12178	20.4	12.77±0.12	-18.78±0.24	87.54±14.56	12.86±0.06	36.31±0.68	23.13±0.12	-0.18±0.12	0.86±0.12	-0.06±0.21	-0.19±0.21
187	A22551p1931	12265	57.9	15.69±0.02	-18.13±0.08	19.65± 2.95	15.79±0.03	4.73±0.04	22.00±0.03	0.05±0.04	1.32±0.03	0.19±0.10	-0.04±0.05
188	NGC7436	12269	75.4	13.25±0.04	-21.14±0.07	80.18±13.46	13.41±0.06	28.11±0.43	23.60±0.10	0.60±0.04	1.65±0.04	-0.11±0.08	-0.13±0.07
189	NGC7460	12312	33.5	13.42±0.01	-19.21±0.13	54.44± 3.76	13.48±0.01	17.04±0.09	22.03±0.03	-0.08±0.02	1.03±0.01	-0.01±0.03	-0.09±0.03
190	NGC7537	12442	27.2	13.78±0.02	-18.39±0.16	41.83± 4.91	13.83±0.01	11.93±0.07	21.98±0.03	-0.01±0.02	1.25±0.02	-0.15±0.04	-0.28±0.04
191	NGC7548	12455	80.3	14.24±0.02	-20.28±0.06	42.24± 2.72	14.32±0.01	13.39±0.15	22.84±0.04	0.53±0.03	1.61±0.02	-0.14±0.04	-0.19±0.04
192	A23176p1541	12519	44.7	14.46±0.01	-18.79±0.10	30.55± 2.08	14.51±0.01	11.98±0.05	22.28±0.03	0.09±0.02	1.28±0.01	-0.22±0.03	-0.31±0.02
193	NGC7620	12520	98.1	13.80±0.01	-21.16±0.04	37.64± 1.95	13.83±0.01	10.07±0.04	21.68±0.02	0.03±0.01	1.13±0.01	-0.21±0.02	-0.28±0.02
194	A23264p1703	12620	69.2	13.49±0.02	-20.71±0.07	61.56± 4.85	13.60±0.02	17.06±0.14	22.94±0.03	0.54±0.02	1.61±0.02	-0.08±0.04	-0.09±0.03
195	IC1504	12734	63.1	14.15±0.02	-19.85±0.07	38.14± 2.97	14.22±0.01	14.53±0.10	22.50±0.04	0.26±0.03	1.47±0.02	-0.17±0.05	-0.31±0.04
196	NGC7752	12779	50.3	14.52±0.03	-18.99±0.09	31.20± 4.78	14.66±0.03	6.49±0.03	21.32±0.03	-0.30±0.03	1.01±0.03	0.23±0.06	0.05±0.06
197	A23514p2813	12835	70.5	14.22±0.05	-20.02±0.08	42.72± 3.20	14.39±0.02	11.02±0.11	22.73±0.03	0.55±0.05	1.61±0.05	-0.01±0.10	-0.09±0.09
198	A23542p1633	12856	19.1	14.29±0.03	-17.11±0.22	43.97± 1.67	14.34±0.02	19.04±0.18	23.19±0.06	-0.16±0.03	0.73±0.03	-0.13±0.06	-0.09±0.06

[†]abbreviated; colour difference measures $\Delta(U-B)_{25-75}$ and $\Delta(B-R)_{25-75}$ are implied.

This figure "fig3_01.gif" is available in "gif" format from:

<http://arxiv.org/ps/astro-ph/9910075v1>

This figure "fig2.gif" is available in "gif" format from:

<http://arxiv.org/ps/astro-ph/9910075v1>

This figure "fig3_02.gif" is available in "gif" format from:

<http://arxiv.org/ps/astro-ph/9910075v1>

This figure "fig3_03.gif" is available in "gif" format from:

<http://arxiv.org/ps/astro-ph/9910075v1>

This figure "fig3_04.gif" is available in "gif" format from:

<http://arxiv.org/ps/astro-ph/9910075v1>

This figure "fig3_05.gif" is available in "gif" format from:

<http://arxiv.org/ps/astro-ph/9910075v1>

This figure "fig3_06.gif" is available in "gif" format from:

<http://arxiv.org/ps/astro-ph/9910075v1>

This figure "fig3_07.gif" is available in "gif" format from:

<http://arxiv.org/ps/astro-ph/9910075v1>

This figure "fig3_08.gif" is available in "gif" format from:

<http://arxiv.org/ps/astro-ph/9910075v1>

This figure "fig3_09.gif" is available in "gif" format from:

<http://arxiv.org/ps/astro-ph/9910075v1>

This figure "fig3_10.gif" is available in "gif" format from:

<http://arxiv.org/ps/astro-ph/9910075v1>

This figure "fig3_11.gif" is available in "gif" format from:

<http://arxiv.org/ps/astro-ph/9910075v1>

This figure "fig3_12.gif" is available in "gif" format from:

<http://arxiv.org/ps/astro-ph/9910075v1>

This figure "fig3_13.gif" is available in "gif" format from:

<http://arxiv.org/ps/astro-ph/9910075v1>

This figure "fig3_14.gif" is available in "gif" format from:

<http://arxiv.org/ps/astro-ph/9910075v1>

This figure "fig3_15.gif" is available in "gif" format from:

<http://arxiv.org/ps/astro-ph/9910075v1>

This figure "fig3_16.gif" is available in "gif" format from:

<http://arxiv.org/ps/astro-ph/9910075v1>

This figure "fig3_17.gif" is available in "gif" format from:

<http://arxiv.org/ps/astro-ph/9910075v1>

This figure "fig3_18.gif" is available in "gif" format from:

<http://arxiv.org/ps/astro-ph/9910075v1>

This figure "fig3_19.gif" is available in "gif" format from:

<http://arxiv.org/ps/astro-ph/9910075v1>

This figure "fig3_20.gif" is available in "gif" format from:

<http://arxiv.org/ps/astro-ph/9910075v1>

This figure "fig3_21.gif" is available in "gif" format from:

<http://arxiv.org/ps/astro-ph/9910075v1>

This figure "fig3_22.gif" is available in "gif" format from:

<http://arxiv.org/ps/astro-ph/9910075v1>

This figure "fig3_23.gif" is available in "gif" format from:

<http://arxiv.org/ps/astro-ph/9910075v1>

This figure "fig3_24.gif" is available in "gif" format from:

<http://arxiv.org/ps/astro-ph/9910075v1>

This figure "fig3_25.gif" is available in "gif" format from:

<http://arxiv.org/ps/astro-ph/9910075v1>

This figure "fig3_26.gif" is available in "gif" format from:

<http://arxiv.org/ps/astro-ph/9910075v1>

This figure "fig3_27.gif" is available in "gif" format from:

<http://arxiv.org/ps/astro-ph/9910075v1>

This figure "fig3_28.gif" is available in "gif" format from:

<http://arxiv.org/ps/astro-ph/9910075v1>

This figure "fig3_29.gif" is available in "gif" format from:

<http://arxiv.org/ps/astro-ph/9910075v1>

This figure "fig3_30.gif" is available in "gif" format from:

<http://arxiv.org/ps/astro-ph/9910075v1>

This figure "fig3_31.gif" is available in "gif" format from:

<http://arxiv.org/ps/astro-ph/9910075v1>

This figure "fig3_32.gif" is available in "gif" format from:

<http://arxiv.org/ps/astro-ph/9910075v1>

This figure "fig3_33.gif" is available in "gif" format from:

<http://arxiv.org/ps/astro-ph/9910075v1>

This figure "fig3_34.gif" is available in "gif" format from:

<http://arxiv.org/ps/astro-ph/9910075v1>

This figure "fig3_35.gif" is available in "gif" format from:

<http://arxiv.org/ps/astro-ph/9910075v1>